Molecular Pharmacology Fast Forward. Published on June 14, 2021 as DOI: 10.1124/molpharm.121.000271
This article has not been copyedited and formatted. The final version may differ from this version.

Molecular Pharmacology

High-throughput screening of TRPV1 ligands in the light of the Bioluminescence Resonance Energy Transfer technique

Yann Chappe[1], Pauline Michel[2], Alexandre Joushomme[1], Solène Barbeau[3,4], Sandra Pierredon[5], Luc Baron[2], André Garenne[1], Florence Poulletier De Gannes[1], Annabelle Hurtier[1], Stanislas Mayer[2], Isabelle Lagroye[1], Jean-François Quignard[3,4], Thomas Ducret[3,4], Vincent Compan[5], Christelle Franchet[2] & Yann Percherancier[1,§]

[1] Bordeaux University, CNRS, IMS laboratory, UMR5218, F-33400 Talence, France
[2] Domain Therapeutics, BIOPARC 1, 850 Boulevard Sébastien Brant, F-67400 Illkirch – France
[3] Univ. Bordeaux, Centre de Recherche Cardio-Thoracique de Bordeaux, U1045, F-33600 Pessac, France
[4] INSERM, Centre de Recherche Cardio-Thoracique de Bordeaux, U1045, F-33600 Pessac, France
[5] IGF, CNRS, INSERM, Univ. Montpellier, F-34094 Montpellier, France

§ Correspondence to yann.percherancier@ims-bordeaux.fr

Downloaded from molpharm.aspetjournals.org at ASPET Journals on March 20, 2024

Molecular Pharmacology Fast Forward. Published on June 14, 2021 as DOI: 10.1124/molpharm.121.000271
This article has not been copyedited and formatted. The final version may differ from this version.

Running Title: HTS screening of TRPV1 using BRET

Correspondence to Yann Percherancier
Laboratoire IMS / UMR5218
Université de Bordeaux I – Bat. A31
351 av de la liberation
F-33400 Talence
France
Tel: 0540002724
Mail: yann.percherancier@ims-bordeaux.fr

31 pages
11 figures
6 supplementary figures
3 tables
4 supplementary tables

Abstract: 207 words
Introduction: 691 words
Discussion: 1417 words

Abbreviations
ACA: Automated calcium assay
APC: Automated patch-clamp
BRET: Bioluminescence Resonance Energy Transfer
CAPS: Capsaicin
CaM: Calmodulin
CPZ: Capsazepine
GPCR: G-protein-coupled receptors
HTS: High-throughput screening
mNeonG: mNeon Green protein
nLuc: nano Luciferase
rLuc2 : Renilla Luciferase 2
RTX: Resiniferatoxin
sYFP2: Yellow super fluorescent protein 2
TRPV1: Transient Receptor Potential channel 1

Downloaded from molpharm.aspetjournals.org at ASPET Journals on March 20, 2024

Molecular Pharmacology Fast Forward. Published on June 14, 2021 as DOI: 10.1124/molpharm.121.000271
This article has not been copyedited and formatted. The final version may differ from this version.

Abstract

Ion channels are attractive drug targets for many therapeutic applications. However, high-throughput screening (HTS) of drug candidates is difficult and remains very expensive. We thus assessed the suitability of the Bioluminescence Resonance Energy Transfer (BRET) technique as a new HTS method for ion-channel studies by taking advantage of our recently characterized intra- and intermolecular BRET probes targeting the TRPV1 ion channel. These BRET probes monitor conformational changes during TRPV1 gating and subsequent coupling with Calmodulin, two molecular events that are intractable using reference techniques such as automated calcium assay (ACA) and automated patch-clamp (APC). We screened the small-sized Prestwick chemical library, encompassing 1200 compounds with high structural diversity, using either intra- and intermolecular BRET probes or ACA. Secondary screening of the detected hits was done using APC. Multiparametric analysis of our results shed light on the capability of calmodulin inhibitors included in the Prestwick library to inhibit TRPV1 activation by Capsaicin (CAPS). BRET was the lead technique for this identification process. Finally, we present data exemplifying the use of intramolecular BRET probes to study other TRPs and non-TRPs ion channels. Knowing the ease of use of BRET biosensors and the low cost of the BRET technique, these assays may advantageously be included for extending ion-channel drug screening.

Significance Statement

We screened a chemical library against TRPV1 ion channel using Bioluminescence Resonance Energy Transfer (BRET) molecular probes, and compared the results with the ones obtained using reference techniques such as automated calcium assay and automated patch-clamp. Multiparametric analysis of our results shed light on the capability of Calmodulin antagonists to inhibit chemical activation of TRPV1, and indicates that BRET probes may advantageously be included in ion channel drug screening campaigns.

Downloaded from molpharm.aspetjournals.org at ASPET Journals on March 20, 2024

Molecular Pharmacology Fast Forward. Published on June 14, 2021 as DOI: 10.1124/molpharm.121.000271
This article has not been copyedited and formatted. The final version may differ from this version.

Introduction

Ion channels are pore-forming membrane proteins allowing ions to flow across membranes. Widely regarded as attractive drug targets for many therapeutic applications, ion channels are the second largest class of membrane proteins for drug discovery behind G protein-coupled receptors (GPCRs). They account for worldwide sales above US$ 18 billion, which highlights their 'tractable' nature (Wickenden *et al.*, 2012; Global data, 2020). Nonetheless, despite its commercial potential and academic relevance, in-vitro pharmacological profiling of most ion channels remains unaddressed (Bagal *et al.*, 2015).

Automated patch-clamp (APC) is rapidly emerging and provides increased throughput screening of ion channel targets (Obergrussberger *et al.*, 2018) but it remains expensive and requires expert handling (Terstappen *et al.*, 2010; Yu *et al.*, 2016). As a consequence, indirect-readout technologies are often used for initial screening to be later confirmed by APC. Generally, these techniques take advantage of fluorescent probes to monitor changes in membrane potential or concentration of cytoplasmic ions such as calcium (Terstappen *et al.*, 2010; Yu *et al.*, 2016; McGivern and Ding, 2020). Such assays give only an indirect readout of channel activity since they monitor molecular mechanisms that are spatially or temporally distant from the studied channel, with the risk that the tested compound could up- or down-modulate non-specific targets. They are therefore prone to a high yield of false positives (Clare, 2010). This drawback can be bypassed by measuring events proximal to the studied ion channel once activated.

For the last twenty years, resonance-energy-transfer (RET) based techniques have revolutionized molecular pharmacology and biochemistry, allowing measurement of protein-protein interaction and protein conformational changes in real-time in live cells (Miyawaki and Niino, 2015). These techniques are based on the nonradiative intra- or inter-molecular transfer of energy between an energy donor and a compatible fluorescent energy acceptor. Such quantum mechanism strictly relies on molecular proximity (around 100 Å) and orientation between donor and acceptor molecules for energy transfer, making it ideal for probing either protein conformational changes or the dynamic of protein-protein interactions. Independence from an external energy source for donor excitation gives Bioluminescence Resonance Energy Transfer (BRET) some advantages over related methods such as Fluorescence Resonance Energy Transfer (FRET), by avoiding cells photodamage, fluorophore photobleaching, background autofluorescence, or direct acceptor excitation (Pfleger *et al.*, 2006). Thanks to these advantages, BRET assays have been widely implemented for GPCR and kinases drug screening (Bacart *et al.*, 2008; Kocan and Pfleger, 2011; Schann *et al.*, 2013; Ayoub, 2016).

Ironically, while ion channels have been perceived as the « next GPCR » for the last 15 years, according to their importance as a drug target (Kaczorowski *et al.*, 2008), they only recently benefited from BRET technology (Robertson *et al.*, 2016; Ruigrok *et al.*, 2017). Such BRET probes monitor molecular events related to ion-channel activation (conformational changes during gating and protein-protein interactions dynamics) that are of utmost importance for ion channel pharmacology while being intractable using either one of the aforementioned reference techniques for ion-channel HTS. They, therefore, opened up new prospects for improving the effectiveness of ion-channel drug screening. Nonetheless, acceptance of intra- and intermolecular BRET assays as novel tools for ion-channel drug screening relies on their efficiency with regards to conventional methods, and need therefore a solid proof-of-concept of their operability and effectiveness under real drug-screening conditions.

Here, we assessed the suitability of the BRET technique as a new HTS method for ion channels by taking advantage of our recently characterized intra- and intermolecular BRET probes targeting TRPV1 conformational changes during gating and subsequent coupling with Calmodulin (CaM), two events leading to TRPV1 activation and regulation (Ruigrok *et al.*, 2017). We then screened the small-sized Prestwick chemical library, encompassing 1200 FDA- and EMA-approved compounds with high structural diversity using either automated calcium assays (ACA) or our intra- and intermolecular BRET probes. We next performed a secondary screen of the detected hits with an automated patch-clamp (APC). Multiparametric analysis of our results put into light the power of the BRET technique to unravel hits compounds that would not have been detected with conventional methods such as ACA and APC. Finally, we present data exemplifying the use of intramolecular BRET probes for the study of other TRPs and non-TRPs ion channels.

Downloaded from molpharm.aspetjournals.org at ASPET Journals on March 20, 2024

Molecular Pharmacology Fast Forward. Published on June 14, 2021 as DOI: 10.1124/molpharm.121.000271
This article has not been copyedited and formatted. The final version may differ from this version.

MATERIALS AND METHODS

Plasmids

The mammalian expression vector encoding sYFP2-TRPV1-rLuc2, TRPV1-rLuc2, and sYFP2-CaM were described in (Ruigrok *et al.*, 2017). To generate the other BRET constructs, mNeonGreen and nanoluciferase were used to improve the brightness of the assay in some experiments, and are referred as mNeonG and nLuc for short in the rest of this paper. Mammalian expression vectors for the expression of the nLuc-ion channel-mNeonG or mNeonG-ion channel-nLuc fusion proteins were constructed using cDNA bricks, obtained by gene synthesis (Genescript, Leiden, The Netherlands), that encode respectively nLuc or mNeonGreen (brick 1), any ion channel described in the text (brick 2), and mNeonGreen or nLuc (brick 3). Using the BsmB1 type IIS enzyme and T4 DNA ligase, the cDNA Bricks were assembled in frame and in the right order into pcDNA3.1(+)-Lac Z vector, which allowed direct visualization of the assembly efficiency using a colorimetric test based on alpha complementation (Sup. Table 1). Briefly, a ligation mix containing 2 µl of T4 DNA ligase buffer 10X, 1 U of BsmBI enzyme, 1 U of T4 DNA ligase, 0.4 mM ATP, 4 mM dithiothreitol, 100 ng of pcDNA3.1(+)-Lac Z vector, and 100 ng of bricks 1 to 3 was subjected to 35 cycles alternating two steps (step 1: 37° C for 1 min, step 2: 25° C for 1 min) before the enzymes were inactivated for 5 min at 55° C. The ligation mix was then used to transform *Escherichia coli* DH5α by thermal shock. The mammalian expression vector for SUR1 subunit is a kind gift from Jean Révilloud (Institut de Biologie Structurale, Grenoble, France) and was co-transfected with KiR6.1 BRET probe at a 1:1 ratio. Mammalian expression vector coding for human Calmodulin (clone ID: OHu22088) is from Genescript and was co-transfected with KCa2.3 at a 4:1 ratio.

Reagents

Olvanil, OLDA, Resiniferatoxin (RTX), AMG517, AMG9810, BCTC, JNJ-17203212, and AMG21629 were all from Tocris (Bristol, UK). Capsaicin (CAPS) and Capsazepine (CPZ) were from Sigma (Lyon, France). Coelenterazine H (Nanolight Technology, Pinetop, AZ, USA) was added to a final concentration of 5 µM. The Prestwick chemical library, a collection of off-patent drugs with high chemical and pharmacological diversity, has been obtained from Prestwick Chemical Inc (llkirch-Graffenstaden, France; https://www.prestwickchemical.com/screening-libraries/prestwick-chemical-library/). Of note, we used the previous version of that library with 1200 compounds. Indeed, this library is regularly updated, by adding new compounds of interest and removing others.

Cell culture and transfections for BRET assays

HEK293T cells were maintained in Dulbecco's modified Eagle's medium - high glucose (Cat. No. D6429; Sigma-Aldrich, St. Louis, MO) supplemented with 10% fetal bovine serum, 100 units.mL^{-1} penicillin, and streptomycin. HuH7 cells were maintained in Dulbecco's modified Eagle's medium low glucose (Cat. No. 31885023; Thermo Fisher Scientific, Waltham, MA USA) supplemented with 1% Glutamax (Cat. No. 35050-038; Thermo Fisher Scientific), 10% fetal bovine serum, 100 units.mL^{-1} penicillin and streptomycin.

For BRET assays performed in 96-well plates, cells were seeded at a density of 500,000 cells in 6-well dishes, twenty-four hours before transfection. Transient transfections were performed using Polyethylenimine (PEI, linear, Mr 25,000; Cat. No. 23966 Polysciences, Warrington, PA, USA) with a PEI/DNA ratio of 4:1, as explained in (Percherancier *et al.*, 2009). For intramolecular BRET assays, HEK293T cells were transfected with 0.1 µg of sYFP2-TRPV1-rLuc2 and 1.9 µg of empty pcDNA3.1(+) vector, while HEK293T cells were transfected with 0.1 µg of TRPV1-rLuc2 expression vector and 1.9 µg of sYFP2-CaM expression vectors for intermolecular BRET assays. Following overnight incubation, transfected cells were detached and resuspended in DMEM w/o red phenol (Cat. No. 21063-029; ThermoFisher Scientific) containing 10% fetal bovine serum and 100 units mL^{-1} penicillin and streptomycin, before being seeded at 10^5 cells per well in 96-well white plates (ref 655083, Greiner Bio One, Courtaboeuf, France). Cells were left in culture for an additional 24 h before being processed for BRET assay.

Downloaded from molpharm.aspetjournals.org at ASPET Journals on March 20, 2024

Molecular Pharmacology Fast Forward. Published on June 14, 2021 as DOI: 10.1124/molpharm.121.000271
This article has not been copyedited and formatted. The final version may differ from this version.

BRET assays in high-throughput conditions were performed in 384-well plates, using either HEK293T cells transfected with TRPV1-rLuc2 and sYFP2-CaM or HuH7 cells transfected with sYFP2-TRPV1-rLuc2. Briefly, on the day of the transfection, HEK293T and HuH7 cells were rinsed, detached, and resuspended at a density of 350,000-375,000 cells/mL in DMEM w/o phenol red (Cat. No. 11880028; ThermoFisher Scientific) supplemented with 1% Glutamax, 5% fetal bovine serum, 100 units mL^{-1} penicillin and streptomycin. Two DNA mix containing either 50 ng/mL of the hTRPV1-rLuc2 expression vector, 200 ng/mL of the sYFP2-Calmoduline expression vector, and 750 ng/mL of non-coding salmon sperm DNA (ssDNA), for the intermolecular BRET assay, or 800 ng/mL of YFP-hTRPV1-Luc expression vector and 200 ng/mL of ssDNA, for the intramolecular BRET assay, were prepared in 150 mM NaCl and mixed with an equal volume of PEI, 3 times more concentrated than total DNA (i.e. 3:1 (w/w) PEI/DNA ratio). The DNA/PEI mix was then incubated for 15 min at room temperature before being added to the corresponding cell suspension at a ratio of 1:10 (v/v). HuH7 cells were then seeded directly into white opaque 384-well microplates (Cat. No. 781080; Greiner Bio-One SAS, Les Ulis, France) at a rate of 20 µL per well, i.e. 7,500 cells per well, and were left in culture for an additional 24 h before being processed for BRET assay. HEK293T cells were seeded into a 75-cm² flask (Cat. No. 15632011; Invitrogen™) and were left in culture for an additional 24 h before being detached, and resuspended in equilibration buffer (NaCl 145 mM, KCl 5 mM, KH_2PO_4 4 mM, $CaCl_2$ 1 mM, $MgSO_4$ 1 mM, Glucose 10 mM, pH7.5) at a density of 750,000 cells mL^{-1}. A 384-well plate was then filled with 20 µL (15,000 cells) of the cell suspension per well and left for equilibration for 1 h at 22° C in the dark before being processed for BRET assay.

BRET measurement in 96-well plates

Following the addition of Coelenterazine H into the Red-phenol free cell culture medium at a final concentration of 5 µM, BRET signals were measured using a multidetector TriStar2 LB942 microplate reader (Berthold Technologies, Bad Wildbad, Germany) and emission filters centered at 540±40 nm for YFP and 480±20 nm for Luc, or 515±40 nm for mNeonGreen and 460±20 nm for nLuc.

The BRET signal was determined by calculating the ratio of the emission intensity measured in the acceptor window ($I_{acceptor}$) over the emission intensity measured in the donor window (I_{donor}), according to Eq.1:

$$\text{(1):} \qquad \text{BRET} = \frac{I_{\text{acceptor}}}{I_{\text{donor}}}$$

Due to the overlapping emission spectra of Luc and YFP, a fraction of the light detected in the YFP filter originates from the Luc emission, resulting in a contaminating signal (Hamdan *et al.*, 2006). In that configuration, the net BRET was therefore defined as the BRET ratio of cells co-expressing Luc and YFP constructs minus the BRET ratio of cells expressing only the Luc construct in the same experiment.

To assess the functionality of the ion channel BRET-based probes, Coelenterazine H was added to the cell culture medium 5 min before the injection of agonists and antagonists and subsequent BRET readings. In these experiments, the maximal quantity of DMSO was 0.3%. All experiments were performed at 37° C and pH 7.4 unless otherwise indicated.

Concentration-response and drug screening using intra- and intermolecular BRET assays in 384-well plates.

Screening of the Prestwick Chemical library was performed at 22°C (intermolecular test) or 37°C (intramolecular test) using a 2-step injection protocol. One minute after the injection of Coelenterazine H in each well (10 µL, 5 µM final) to initiate the bioluminescent reaction catalyzed by the Luciferase enzyme, 10 µL of the tested compounds (15 µM final) or vehicle alone was injected to assess each compound ability to activate TRPV1 (hereafter designed as “activation mode”). BRET measurements were performed 5 min (intermolecular BRET assay) or 15 min (intramolecular BRET assay) after compound injection using an EnVision Multimode Plate Reader (Perkin Elmer, Villebon-sur-Yvette, France) with emission filters centered at 535±15 nm for YFP ($I_{acceptor}$) and 480±15 nm for Luc (I_{donor}).

Downloaded from molpharm.aspetjournals.org at ASPET Journals on March 20, 2024

Molecular Pharmacology Fast Forward. Published on June 14, 2021 as DOI: 10.1124/molpharm.121.000271
This article has not been copyedited and formatted. The final version may differ from this version.

Immediately after this first BRET measurement, 20 µL of the prototypic agonist Capsaicin (CAPS) (final concentration: 500 nM) was injected in each well to assess the ability of each compound to inhibit chemical activation of TRPV1 (hereafter designed as "inhibition mode"). A second BRET measurement was then performed after CAPS injection. In the inhibition mode, the final concentration of the tested compound was 10 µM.

The data in the activation mode are expressed according to Eq.2 and data in the inhibition mode are expressed according to Eq.3.

(2): $$\%\text{ of CAPS effect}=100\times\left(\frac{BRET_{comp}\text{-}BRET_{base}}{BRET_{CAPS\,max}\text{-}BRET_{base}}\right)$$

(3): $$\%\text{ of inhibition}=\left(\frac{BRET_{comp}\text{-}BRET_{CAPS\,EC80}}{BRET_{base}\text{-}BRET_{CAPS\,EC80}}\times 100\right)$$

where $BRET_{comp}$ is the net BRET in the presence of the compound, $BRET_{base}$ is the basal BRET before injection of the compounds, $BRET_{CAPS\ EC80}$ and $BRET_{CAPSmax}$ are the net BRET measured in presence of 500 nM and 15 µM Capsaicin respectively. Two independent runs (n1 and n2) were performed and an arbitrary percent activation or inhibition cut-off of 30% was chosen to select hit-compounds. A counter screen was performed using HEK293T cells transfected with TRPV1-rLuc2 alone. The compound effects on TRPV1 intra- and intermolecular BRET probes were validated only if the basal BRET of TRPV1-rLuc2 remained unaffected during the counter screen step.

In all experiments performed in 384-well plates, the final quantity of DMSO was 1% in the activation mode and 0.87% in the inhibition mode. Reference compounds effects were assessed both in the activation and inhibition modes using identical protocols, except that concentration-responses curves were performed instead of a single concentration measurement. All injection steps were done using a TECAN EVO Freedom 150 Platform (TECAN, Männedorf, Switzerland).

Automated Calcium assay

Automated calcium assays were outsourced to Eurofins Pharma Discovery Services (St. Charles, MO USA). Briefly, HEK293 cell line stably expressing human TRPV1 (Eurofins Cat #CYL3063) were plated in 384 well plates in maintaining medium and incubated at 37 °C and 5% CO_2. After 24 h, the medium was aspirated from the 384 wells and 40 µl of Dye Loading Buffer (Hanks Balanced Salt Solution (HBSS) supplemented with 20 mM HEPES pH 7.4, 2.5 mM Probenecid, and 5 µg/mL Fluo-8 Ca^{2+} Dye) was added to the cells in each well. The assay plate was incubated at 30 °C and 5% CO_2 in a humidified chamber for at least 80 min prior to washing and addition of the FLIPR Assay buffer (HBSS supplemented with 20 mM HEPES, pH 7.4). The calcium flux assays were performed on a Molecular Devices' FLIPR^{Tetra} plate reader (San Jose, CA USA) using an excitation filter centered at 482.5±12.5 nm and an emission filter centered at 545±30 nm. Concentration-response curves were obtained in duplicate by either injecting increasing concentrations of the indicated reference agonist compounds or by injecting increasing concentration of the indicated reference antagonist compound followed, 3 min later, by an injection of 0.1 µM CAPS. Single-point screening of the Prestwick Chemical library was performed using an initial injection of the tested compounds at a final concentration of 15 µM, to assess each compound's ability to activate TRPV1 for 180 s, followed by a second injection of 0.1 µM CAPS, to assess each compound's ability to inhibit CAPS-activated TRPV1 for another 180 s. In the inhibition mode, the final concentration of the tested compound was 10 µM. The compound wells, reference agonist, reference antagonist, and background vehicle controls were prepared in DMSO at 0.44% final in the activation assay and 0.33% final in the inhibition assay. Two independent experiments were performed on all duplicate tests. All plates were subjected to appropriate baseline corrections. Once baseline corrections were processed, maximum fluorescence values were exported to calculate the normalized Ca^{2+} flux relatively to CAPS activation according to Eq. 4:

(4): $$\text{normalized } Ca^{2+}\text{flux}=\frac{RFU_{max}\text{-}Baseline_{avg}}{RFU_{CAPS}\text{-}Baseline_{avg}}$$

Downloaded from molpharm.aspetjournals.org at ASPET Journals on March 20, 2024

where RFU_{max} and $Baseline_{avg}$ are the maximal fluorescence signal and the baseline signal measured during the recording session of the tested compound respectively, and RFU_{CAPS} is the maximal fluorescence signal measured with either 4 µM CAPS (activation mode) or 0.1 µM CAPS (inhibition mode).

In the activation mode, the results are expressed as % of CAPS effect according to Eq.5:

(5): $$\%\ \text{of CAPS effect} = \text{normalized } Ca^{2+} \text{ flux} \times 100$$

In the inhibition mode, the % of inhibition induced by a compound is given by Eq.6:

(6): $$\%\ \text{of inhibition} = 100 - (\text{normalized } Ca^{2+} \text{ flux} \times 100)$$

Manual patch-clamp

For whole-cell electrophysiological study, transiently transfected HEK293T cells were bathed in an extracellular medium containing 135 mM NaCl, 5 mM CsCl, 1 mM $MgCl_2$, 1 mM $CaCl_2$, 10 mM Glucose and 10 mM HEPES. The osmolarity (measured with a cryoosmometer type 15 Löser) of the external salt solution was adjusted to 300 mOsm with Mannitol and pH adjusted to 7.4 with NaOH. The recording patch-clamp pipette was filled with artificial intracellular saline containing: 130 mM CsCl, 5 mM EGTA, 5.5 mM $MgCl_2$, 5 mM Na_2ATP, and 5 mM HEPES (290 mOsm adjusted with Mannitol and pH 7.2 adjusted with NaOH).

Cells were viewed under phase contrast using a Nikon Diaphot inverted microscope. Borosilicate glass micropipettes (GC150F-10, Harvard Apparatus, Phymep, Paris, France) were pulled with a DMZ-Universal puller. The pipettes had a mean resistance of 4 MΩ when measured under standard recording conditions. An RK-400 patch-clamp amplifier (Biologic, Claix, France) was used for whole-cell recordings. Stimulus control, data acquisition, and processing were carried out on a PC fitted with a Digidata 1200 interface, using the pCLAMP 10.7 software (Molecular Devices, Foster City, CA). Current records were filtered using a Bessel filter at 1 kHz and digitized for storage and analysis. Recordings were performed in voltage-clamp and whole-cell configurations to measure global currents. After the seal, a resting potential of –60 mV was imposed and 650 ms voltage ramps from –60 to +60 mV were applied every 10 sec for 3 min. After 4 ramps, Capsaicin (10 µM) was applied to the recorded cell by pressure ejection from a glass pipette located close to the cell. Capsaicin-activated currents were determined by the difference between maximal capsaicin-induced and average current before ejection. Currents were then normalized to cell capacitance and expressed as pA/pF.

Automated Patch-clamp assay

Automated patch-clamp assays were outsourced to SB Drug discovery (Glasgow, UK). Briefly, automated patch-clamp recordings were performed using the SyncroPatch 384PE (Nanion, Munich, Germany) and HEK293 cell line stably expressing human TRPV1 (SB Drug Discovery) that were plated 24 h before the experiment and incubated at 37°C and 5% CO_2. The voltage protocol generation and data collection were performed with the PatchController384 V1.6.6 and Data Controller V1.6.0. Concentration-response curves were obtained by injecting either increasing concentrations of the indicated reference agonist compounds or by injecting increasing concentration of the indicated reference antagonist compound followed 3 min later by an injection of 0.1 µM CAPS. Screening of the Prestwick Chemical library was performed with two different protocols to assess the ability of 10µM concentration of a test compound to either activates TRPV1 (activation mode) or to inhibits CAPS-activated TRPV1 (inhibition mode).

Activation Mode: The protocol consisted of two applications (control period) of an external solution containing 140 mM NaCl, 4 mM KCl, 2 mM $CaCl_2$, 1 mM $MgCl_2$, 10 mM HEPES and 5 mM Glucose, at pH 7.4, followed by the addition of 10 µM of the test compound (1-2 minutes). Then a maximum concentration of agonist (3-10 µM Capsaicin) was added to confirm the presence of the TRPV1 channel and lastly, addition of the full block with 10 µM Capsazepine (1 min) was done. Data points that did not fulfill these controls were discarded. Data were normalized according to Eq.7:

Downloaded from molpharm.aspetjournals.org at ASPET Journals on March 20, 2024

Molecular Pharmacology Fast Forward. Published on June 14, 2021 as DOI: 10.1124/molpharm.121.000271
This article has not been copyedited and formatted. The final version may differ from this version.

(7): $$\% \text{ of CAPS effect} = 100 \times \left(\frac{I_{comp} - I_{base}}{I_{max} - I_{base}}\right)$$

where I_{comp} is the current in the presence of the compound, I_{base} is the baseline current and I_{max} is the max current, in the presence of the maximum concentration of compound or Capsaicin. The concentration-response curves are constrained between 0 (no activation) and 100 (maximum activation).

Inhibition Mode: The protocol consisted of two applications of external solution (control period), one application of the agonist Capsaicin EC_{50} (50 nM) for 1-2 minutes, followed by addition of 10 µM of the test compound (1-2 minutes), in the presence of Capsaicin EC_{50}, and lastly addition of 10 µM Capsazepine (1 minute) to control for full inhibition. Data were expressed as % of inhibition according to Eq.8:

(8): $$\text{normalized } Current = 100 - \left(\frac{I_{comp} - I_{base}}{I_{ref} - I_{base}} \times 100\right)$$

where I_{comp} is the current in the presence of the compound, I_{base} is the baseline current and I_{ref} is the current in the presence of the Capsaicin EC_{50}. The concentration-response curves are constrained between 0 (no inhibition) and 100 (maximum inhibition).

In both activation and inhibition mode, the current was monitored using a ramp protocol from –100 mV to +100 mV over 300 ms, from a holding potential of –60 mV, which was repeated every 20 s. The maximum outward current at +100 mV was used for analysis. In each condition, the maximum DMSO concentration at the end of the run was 0.3%.

Data preparation, normalization, analysis, and statistics

GraphPad Prism v6.00 for Windows (GraphPad Software, La Jolla, CA, USA) was used for plotting concentration-response curves. The size of the error bars indicates the standard deviation (SD) within the data set. Potencies of chemicals to activate or inhibit TRPV1 are expressed as pEC_{50}±S.E. (-Log EC_{50}±standart error).

Scatter plots, histograms, radar charts, and whisker boxes were plotted using the ggplot2 R package. Statistical analyses were performed using Anastats (Rilly sur Vienne, France), R, and the PMCMRplus R package. Multiple comparisons were performed using Kruskal-Wallis and Conover posthoc tests.

Hierarchical cluster analysis was performed using R and the dplyr, ggplot2, factorextra, and NbClust libraries (Charrad *et al.*, 2014; Wickham, 2016; Kassambara and Mundt, 2020; R Core Team, 2020; Wickham *et al.*, 2020).

Hierarchical Agglomerative Clustering (HAC) is a multivariate statistical classification method of cluster analysis which aim is to build a hierarchy of clusters according to the similarity or the dissimilarity of their characteristics. It is an exploratory approach which interpretation depends on the experimental context. Here, the clustering was performed on 54 of the 59 identified hits-compounds (see results) and applied to the characteristics listed in table 1.

The values were first normalized (mean-centered and scaled) and an optimal number of clusters was automatically assessed using the NbClust package giving an optimal number of 7 clusters. To compute the NbClust algorithm we used maximum distance and complete-linkage method which are often preferred and tend to produce more compact clusters.

Hierarchical cluster analysis was applied using the complete-linkage method. Three analyses were performed: one relying on the 12 parameters (Table 1), one without the intra and intermolecular BRET measures, and one without the fluorescent probe-based calcium measurements. The clustering results were then visualized with dendrograms.

Downloaded from molpharm.aspetjournals.org at ASPET Journals on March 20, 2024

Molecular Pharmacology Fast Forward. Published on June 14, 2021 as DOI: 10.1124/molpharm.121.000271
This article has not been copyedited and formatted. The final version may differ from this version.

Results

Comparison of the capability of both intra- and intermolecular BRET probes, automated calcium assay, and automated patch-clamp to measure the potency and efficacy of reference compounds.

We first addressed whether both intra- and intermolecular BRET biosensors discriminate between known TRPV1 agonists and antagonists that are expected to display different potencies. In these experiments, HEK293T cells transiently expressing either the intramolecular BRET probe sYFP2-TRPV1-rLuc2 (Fig. 1A) or the BRET pair TRPV1-rLuc2 / sYFP2-CaM (Fig. 1B, intermolecular BRET assay), and plated in 96-well plate, were first challenged with increasing quantities of four known TRPV1 agonists. As expected, both CAPS, RTX, OLDA, and Olvanil induced a concentration-dependent increase of intra- (Fig. 1A) and intermolecular (Fig. 1B) basal BRET. CAPS, Olvanil and RTX maximally increased the TRPV1 intramolecular BRET ratio by 50% from 0.5 to 0.75 (Fig. 1C), and the TRPV1 intermolecular BRET ratio by 700% from 0.05 to 0.35 (Fig. 1D). While the absolute variation of the BRET ratio was similar and highly significant for both assays (0.25 for the intramolecular BRET assay and 0.3 for the intermolecular assay), the relative increase was lower when considering the TRPV1 intramolecular BRET probe. This is easily explained by a higher basal BRET ratio for the intramolecular BRET probe, which is expected given the proximity of N- and C-terminus extremities in the tetrameric quaternary structure of TRPV1 ion channels (De-la-Rosa *et al.*, 2013). In sharp contrast, since CaM is only weakly coupled to TRPV1 in the resting state (Hasan *et al.*, 2017; Ruigrok *et al.*, 2017), the intermolecular basal BRET ratio is very low, leading to bigger relative changes following activation. In agreement with others, we found that OLDA maximal efficacy was lower than CAPS to activate human TRPV1 in transfected HEK293 cells (Bianchi *et al.*, 2006). The rank order of EC_{50} values for each agonist was conserved for both BRET biosensors and is in full agreement with the literature (Winter *et al.*, 1990; Ralevic *et al.*, 2001; Bianchi *et al.*, 2006) with RTX > CAPS ~ Olvanil > OLDA (Fig.1 and Table 2).

We, therefore, assessed the efficacy and potency of various TRPV1 antagonists using our intra- and intermolecular BRET probes. As shown in Fig. 1E & Fig. 1F, using both intra- and intermolecular TRPV1 BRET probes, we confirmed that Capsazepine (CPZ), AMG519, AMG9810, BCTC, JNJ-17203212, and AMG21629 fully antagonized TRPV1 activation by CAPS (hereafter noted TRPV1(CAPS)) in agreement with the literature (Gavva *et al.*, 2005; Swanson *et al.*, 2005; Bianchi *et al.*, 2006; Narender R. Gavva *et al.*, 2007; N. R. Gavva *et al.*, 2007; Papakosta *et al.*, 2011). However, using both BRET assays, the antagonist SB366791 was found to only partially antagonize TRPV1(CAPS), which is in contradiction with the initial characterization of this compound as a full antagonist (Gunthorpe *et al.*, 2004). We however confirmed that SB366791 is a weak antagonist (Table 2). As expected, RN1734, which is known to be a TRPV4 specific antagonist failed to inhibit TRPV1(CAPS). These results indicate that both TRPV1 intra- and intermolecular BRET assays are fully functional to assess the agonist and antagonist behavior of chemical compounds. This statement is reinforced by the fact that both the shape of the I/V curve and the magnitude of the outward current flowing through both untagged TRPV1 and TRPV1 intramolecular BRET probe are similar in transiently transfected HEK293T cells challenged with CAPS (Sup. Fig. 1). This further supports our previous observations that N- and C-terminal addition of either the YFP and/or Luc groups does not hinder TRPV1 activity (Ruigrok *et al.*, 2017).

The acceptance of BRET probes as a novel tool for ion-channel drug screening relies on their operability and effectiveness with regards to conventional methods. We, therefore, performed concentration-response curves of the aforementioned TRPV1 agonists and antagonists using HTS-platforms for both automated-patch clamp (APC) and fluorescent probe-based calcium measurement. The resulting potency of these chemicals to modulate TRPV1 activity were compared with the ones measured using our intra- and intermolecular BRET assays in the 384 well plate format. As shown in Fig. 2 and Table 2, the potency measured using each technique was in a similar range for the four agonists tested. Considering the data obtained with the antagonist compounds, we found that the pIC_{50} measured with both intramolecular and intermolecular BRET probes were again close to the ones measured with the automated calcium assay (ACA). APC yielded however significantly better pIC_{50}

Downloaded from molpharm.aspetjournals.org at ASPET Journals on March 20, 2024

than the ones measured with either BRET probes or ACA for five antagonists out of the seven tested. Knowing that the classical concentration of compounds tested in a primary high-throughput screening usually lies between 1 and 10 µM, our results indicate however that both TRPV1-based BRET assays are as fit to perform high-throughput screening as the conventional APC and automated Ca^{2+}-flux methods.

Assessment of technical and biological reproducibility for both intra- and intermolecular BRET assays.

We next assessed the suitability of our BRET assays for HTS purposes using transfected cells seeded in 384-well plates. We first assessed the technical and biological reproducibility of both intra- and intermolecular BRET assays by comparing the results of two independent experiments (done on two different days) where CAPS concentration-response curves were obtained on four consecutive 384-well plate assays (Fig. 3). All concentration-response curves fitting into the range of three standard deviations (3SD), our results indicated that both TRPV1 intra- and intermolecular assays offered good biological and technical reproducibility (Fig. 3A&B). To determine the Z'-factor of the assay (Zhang *et al.*, 1999), we measured the efficacy of 500 nM CAPS to trigger TRPV1 conformational change and Calmodulin coupling over five independent experiments performed over three different days with 16-24 wells measured per plate (Fig. 3C&D). All calculated Z'-factor were above or close to 0.5 indicating that both intra- and intermolecular assays for TRPV1 were of high quality and suitable for HTS (average Z'-factor were 0.58±0.04 (average±S.E.) and 0.54±0.04 for intra- and intermolecular BRET assays, respectively).

The primary screen of the Prestwick Chemical Library for TRPV1 activation and inhibition.

Based on this conclusion, we used HTS experimental conditions with ACA and both intra- and intermolecular BRET probes to screen the Prestwick Chemical library for both activation (Fig. 4) and inhibition (Fig. 5) of TRPV1. The final drug concentration was 15 µM during the measurement of the compound efficacy to activate TRPV1 and was 10 µM during the measurement of the compound efficacy to inhibit TRPV1 activation following the injection of 500 nM CAPS (which is close to CAPS EC_{80} in our experimental condition, e.g., the concentration of CAPS inducing 80% of TRPV1 maximal activation). Two independent runs (n1 and n2) were performed and an arbitrary percent activation or inhibition cut-off of 30% was chosen to select hit-compounds. As expected, most compounds exhibited little to no effect whatever the assay considered, while a small percentage of compounds demonstrated positive or negative modulation of TRPV1 activity in either activation or inhibition modes (Fig. 4A-C, Fig. 5A-C & supplementary Table 2). Interestingly, when plotting the compounds' percent distribution histograms, data from BRET experiments exhibited distribution profiles different than data issued from the Ca^{2+} flux method. The latter displayed an asymmetric profile with a significantly broader basis, especially in the inhibition mode (Fig. 4D-F and Fig. 5D-F). Reproducibility between the results obtained during the two independent runs was derived from scatter plots analysis (Fig. 4G-H, & Fig. 5G-H) using different statistical methods. Firstly, the median distance between each experimental dot and a theoretical perfect duplicate assay was computed and compared between the three methods used (intramolecular BRET probe, intermolecular BRET probe, and ACA) for both activation and inhibition modes (Sup. Fig. 2). We found that data dispersion was significantly lower for the intermolecular BRET probe than for the two other techniques in the activation mode and significantly lower for both intra- and intermolecular BRET assays in comparison to the results obtained with ACA in the inhibition mode. Secondly, the global dispersion of the pooled data (n1 and n2) was estimated using 4 classical dispersion metrics: the median absolute deviation (mad), the difference between the largest and smallest values (range), the quartile coefficient of dispersion (qcod) and the interquartile range (iqr). For all these four metrics, the radar chart area is proportional to the data dispersion. As shown in Sup. Fig. 3, the calcium-activated method exhibited a much larger area compared to values obtained from the two BRET assays, pointing toward a higher overall signal values dispersion of ACA. The overall conclusion is that TRPV1 BRET probes provide a statistically better signal reproducibility than ACA in high-throughput screening conditions. Accordingly, we found a significantly higher percentage of confirmed hits between both

Downloaded from molpharm.aspetjournals.org at ASPET Journals on March 20, 2024

Molecular Pharmacology Fast Forward. Published on June 14, 2021 as DOI: 10.1124/molpharm.121.000271
This article has not been copyedited and formatted. The final version may differ from this version.

replicate assays in the activation mode when using intra- or intermolecular BRET probes (100% and 87.5% of confirmed hits, respectively) in comparison to the calcium assay for which we found 18.1% of confirmed hits (Table 3). While the percentage of confirmed hits was lower in the inhibition mode than in the activation mode for all three assays, the percentage of confirmed hits for both intra- and intermolecular BRET probes (42.6% and 58.8%, respectively) was still higher than the one found for the calcium assay (31.2%). This confirms that both BRET assays are sufficiently fit for reliable hit identification.

Hit confirmation with APC.

The Venn diagrams in Fig. 6 show the total number of unique hits detected by each assay in the activation mode (Fig. 6A) and the inhibition mode (Fig. 6B). A total of 22 compounds were shown to reproducibly trigger TRPV1 in both replicate screens while 47 compounds were shown to reproducibly inhibit TRPV1(CAPS). Remarkably, only three hits were common to the three methods when regarding the inhibition mode (Thioridazine hydrochloride, Perphenazine, and Benzethonium chloride) while no hits were common to the three methods when regarding the activation mode. Two hits were detected by both intermolecular and calcium assay to activate TRPV1. Considering the inhibition mode, one hit was common to both calcium assay and intermolecular BRET probe, two hits were common to both intramolecular BRET probe and calcium assay and four hits were common to both intra- and intermolecular BRET probes. Since 10 compounds were identified in at least two different tests, all assays combined, this primary screen, therefore, identified a total of 59 hits (4.9 % of the bank).

We then re-assessed the efficacy of each of these 59 compounds to activate TRPV1 or inhibit TRPV1(CAPS) using automated patch-clamp assay (APC). In a preliminary step, we first confirmed that TRPV1 behaved as an outwardly rectifying channel when stably expressed in HEK293T cells, as already described by others in several primary cells and cell lines (Caterina *et al.*, 1997; Tominaga *et al.*, 1998; Premkumar *et al.*, 2002)(Fig. 7A). Knowing the outward rectifying properties of TRPV1, it is important to emphasize that most electrophysiologists assess TRPV1 activity by measuring the outward potassium current flowing through the TRPV1 ion channel at high positive membrane potential (e.g. between +60 and +100 mV). The reason is that, while this outward current measured at high positive membrane potential is less physiologically relevant, it is of much greater amplitude than the inward current measured at the negative resting membrane potential of cells (B.T. Priest *et al.*, 2007). During a drug screening, the implicit assumption for such practice is that any hit displays an equal ability to activate or inhibit TRPV1 gating irrespective of the membrane potential. We, therefore, compared CAPS and CPZ potency to activate or inhibit TRPV1 ion channel when cell membrane potential was clamped at +100 mV, –25 mV (which is the resting membrane potential of HEK293T cells (Kirkton and Bursac, 2011)) and –100 mV. As shown in Fig. 7B, CAPS potency was right shifted when the membrane potential was shifted from +100 mV to –25 mV and remained identical between –25 mV and –100 mV. CPZ potency to antagonize TRPV1 gating by CAPS was similar between +100 mV and –25 mV but was right shifted at –100 mV (Fig. 7C). These results indicated that the membrane potential impacts CAPS and CPZ potency to activate or inhibit TRPV1. By the way, they provided a potential explanation for the difference in apparent potency of some TRPV1 reference agonists and antagonists measured with either APC, BRET probes, or ACA (Fig. 1 & 2), and called for an in-depth analysis of the efficacy of the 59 identified compounds to activate or inhibit TRPV1 gating as a function of the applied membrane potential during APC experiments.

Among the 59 compounds tested, 5 compounds known to be detergent molecules induced a high non-specific current in untransfected HEK293T cells (Chlorhexidine (#10), Methyl benzethonium chloride (#38), Benzethonium chloride (#39; which one was initially identified by all methods), Alexidine dihydrochloride (#42), Thonzonium bromide (#49)) and were discarded from the rest of the study (Sup. Table 3). Assessment of the ability of the 54 remaining drugs to either activate TRPV1 or inhibit TRPV1(CAPS) indicated a strong disparity between the results measured at –100 mV, –25 mV, and +100 mV (Fig. 7 C&D). Only six compounds were shown to be confirmed as TRPV1 activator by APC at +100 mV, with a cut-off of 30% of CAPS efficacy (Fig. 7C). Among these six compounds, only two (compounds 40 and 47) were detected whatever the voltage used. Interestingly, compound 27 was found to activate TRPV1 very efficiently at +100 and –100 mV but not at –25 mV. Also, compounds 29 and 58 did not activate TRPV1 at +100 and –25 mV while they did it at –100 mV. Eleven compounds

Downloaded from molpharm.aspetjournals.org at ASPET Journals on March 20, 2024

Molecular Pharmacology Fast Forward. Published on June 14, 2021 as DOI: 10.1124/molpharm.121.000271
This article has not been copyedited and formatted. The final version may differ from this version.

inhibited CAPS-induced TRPV1 activation at +100 mV but only three of them inhibited TRPV1 activation by CAPS whatever the voltage used (compounds 20, 32, and 58) (Fig. 7D). Compounds 22, 30, and 48 partially blocked TRPV1 activation by CAPS at +100 mV but displayed no inhibitory activity at either –25 mV or –100 mV. Compound 19 efficiently inhibited TRPV1-CAPS activation at +100 mV but potentiated CAPS-activation at –25 mV and had no effect at –100mV. Compound 60 was as efficient as CPZ to antagonize CAPS activation of TRPV1 at both +100 and –25 mV but potentiated CAPS activation at –100 mV. Compound 55 behaved as a partial antagonist of TRPV1 activation by CAPS at –25 and –100 mV but had no effect at +100 mV. Compound 31 potentiated TRPV1 activation by CAPS at –100 mV but had no effect at either –25 mV or +100 mV. Finally, compound 40 (not represented on Fig 7C for simplification) strongly potentiated CAPS activation whatever the voltage considered (% of CPZ effect was –343.2, –52.4, and –95.75 respectively for +100 mV, –25 mV, and –100 mV). Altogether, these results indicate that, when using APC, the behavior of a given compound to modulate an ion channel can vary drastically depending on the plasma membrane potential.

Correlation between chemical structure-driven and data-driven clustering points to Calmodulin antagonists as TRPV1 inhibitors.

Since no consensus emerged from the comparison of the results obtained with each assay taken independently, we next performed a structure-driven and a data-driven clustering of these 54 drugs to unravel a potential structure-function relation that might, in the light of the bibliography, provide insights into the ability of each drug to either activate or inhibit TRPV1.

We found that all 54 identified-drugs could be sorted in only 11 different clusters (Sup. Table 3). Cluster A contains drugs harboring a trifluoromethyl benzene group. Cluster C contains drugs harboring a bicycle in their structure. Cluster D is composed of detergent molecules. Cluster E is composed of molecules with at least three aromatic moieties joined by at least a carbon-carbon single bond, while cluster F contains drugs with only two aromatic rings joined by a linker. Cluster G contains tricyclic compounds such as phenothiazines. Cluster H, I, J, and S contain macrocyclic lactones, statins, dihydropyridines, and sterols-derived compounds respectively. Finally, 5 compounds did not fit in any of the aforementioned clusters and belong therefore to a miscellaneous cluster.

We next performed hierarchical clustering of the data acquired with these 54 hits, taking into account the 12 parameters integrating the results measured with both intra- and intermolecular BRET probes, ACA and APC at +100 mV, –25 mV, and –100 mV in both activation and inhibition modes. The resulting dendrogram (Fig. 8) indicates the correspondence with the aforementioned structure-driven clustering and the measured activity of the drug as assessed with each technique in both activation and inhibition mode.

The most important correlation arising from this multiparametric analysis points to a significant enrichment of drugs belonging to clusters E, G, and J into group 7 of the dendrogram (Sup. Fig. 4). This prompted us to perform an in-depth analysis of the literature focusing on these clusters. Strikingly, we found that 12 of the 24 hits belonging to cluster E, G, and J are well-known calmodulin antagonists (Trifluopromazine (#01), Chlorpromazine (#03), Thioridazine (#04); Cyproheptadine (#05); Perphenazine (#06), Loperamide (#11), Clotrimazole (#18), Perhexiline maleate (#20), Quinacrine (#22), Fluphenazine (#23), Felodipine (#28), Prenylamine Lactate (#32)) (Rochette-Egly *et al.*, 1982; Johnson and Wittenauer, 1983; Mannhold *et al.*, 1987; Montero *et al.*, 1991; Caldirola *et al.*, 1992; Hegemann *et al.*, 1993; Xin and Zhang, 1993; Oláh *et al.*, 2007; Lübker and Seifert, 2015).

Cluster J contains 3 compounds (Felodipine (#28), Lacidipine (#33), and Cilnidipine (#56)) that are all derived from 3,5-diester-4-aryldihydropyridin and differ by structural variations on ester functions and aryl ring. All these three compounds were shown by the intramolecular BRET probe to antagonize the conformational changes occurring in TRPV1 following CAPS-activation. No effects were detected using any other technique, except for APC at –25 mV that also measured an antagonist effect of Lacidipine (Fig. 8 and Sup. Table 3). To the best of our knowledge, among these three compounds, only Felodipine has been reported to inhibit CaM (Johnson and Wittenauer, 1983). However, due to their similar chemical structure, it is highly possible that both Lacidipine and Cilnidipine, two Ca^{2+} channel blockers (Micheli *et al.*, 1990; Chandra and Ramesh, 2013), also act as CaM antagonists.

Downloaded from molpharm.aspetjournals.org at ASPET Journals on March 20, 2024

Molecular Pharmacology Fast Forward. Published on June 14, 2021 as DOI: 10.1124/molpharm.121.000271
This article has not been copyedited and formatted. The final version may differ from this version.

Nine out of the ten compounds belonging to cluster G are antipsychotropic drugs derived from phenothiazine (Triflupromazine (#01), Chlorpromazine (#03), Thioridazine (#04), Perphenazine (#06), Quinacrine (#22), fluphenazine (#23), Metixene (#30), Methotrimeprazine (#44), and Thiethylperazine maleate (#54)). Phenothiazines are among the most potent calmodulin inhibitors, especially when the phenothiazine derivative is substituted by a halogen (Rochette-Egly *et al.*, 1982; Caldirola *et al.*, 1992). The tenth compound of the cluster G, Cyproheptadine (#05), which is not a phenothiazine, has been described as a Calmodulin inhibitor in one study (Xin and Zhang, 1993) and is structurally related to Amitriptyline, a known Calmodulin inhibitor (Hugh Reynolds and Claxton, 1982). To the best of our knowledge, among the ten compounds belonging to cluster G, the only compounds for which CaM antagonist activity has not been established are Metixene (#30), Methotrimeprazine (#44), and Thiethylperazine maleate (#54) (Volpi *et al.*, 1981; Prozialeck and Weiss, 1982; Rochette-Egly *et al.*, 1982; Oláh *et al.*, 2007; Lübker and Seifert, 2015).

Nine of the twelve compounds belonging to cluster E are composed of poly-cycle rings-containing molecules. Interestingly, Perhexilin maleate (#20) and Prenylamine Lactate (#32) that had been detected as inhibitors by intramolecular BRET probe in the primary screen are both Calmodulin antagonists (Caldirola *et al.*, 1992), and have been confirmed as inhibitors of CAPS-induced TRPV1 activation by APC whatever the voltage used (Fig. 8 and Sup. Table 3). Fluspirilen (#48), which triggered a conformational change in TRPV1 and was detected as an inhibitor by APC +100 mV, is known to bind CaM (Butts *et al.*, 2013) and is structurally related to Penfluridol, a first-generation neuroleptic shown to be a CaM antagonist (Lübker and Seifert, 2015). Butocunazole (#25), which has been detected as an inhibitor of TRPV1(CAPS) by the intramolecular BRET probe is an imidazole-derived compound. Direct interaction of imidazole-derived compounds with Calmodulin has been suggested as a possible mechanism for their antifungal activity (Hegemann *et al.*, 1993; Breitholtz *et al.*, 2020), further suggesting a functional link between CaM inhibition and TRPV1 activation. Sertindole (#35), which contains a 4-piperinyl moiety connected in position 3 of an indole ring, and Astemizole (#08), which contains a 4-amino-piperinyl moiety connected in position 2 of a benzimidaole ring, share structural features with the Calmodulin antagonist CGS 9343B (Norman *et al.*, 1987). Loperamide (#11), a synthetic piperidine derivative, known to inhibit TRPV1 activation by ACA, is a recognized CaM antagonist (Merritt *et al.*, 1982) and can prevent Capsaicin-induced thermal allodynia in primates, in the absence of thermal antinociceptive effects (Butelman *et al.*, 2004). Clotrimazole (#18) has a blurred profile since it was detected as an activator of TRPV1 by the intermolecular BRET probe and APC and inhibitor by intramolecular BRET probe and ACA. Nonetheless, clotrimazole (#18) is a potent Calmodulin inhibitor (Montero *et al.*, 1991; Hegemann *et al.*, 1993) and has been detected as a TRPV1 activator (Meseguer *et al.*, 2008). Of note, clotrimazole-derived compounds are weak competitive inhibitors of TRPV1(CAPS) (Oláh *et al.*, 2007).

To the best of our knowledge, the only hit compound which has been shown to inhibit purified CaM in vitro (Schaeffer *et al.*, 1987) and which does not belong to clusters E, G, or J is Nicergoline (#12), a nitrogen polyheterocyclic compound filed in the miscellaneous cluster (Sup. Table 3). In agreement with these considerations, most CaM inhibitors or putative CaM inhibitors belong to group 7 of the data-driven hierarchical clustering (Fig. 8). Interestingly, the cross-correlation between chemical structure-driven and data-driven clustering indicates that group 7 is mainly composed of drugs initially identified by intra- and/or intermolecular BRET probes (Fig. 8). Hierarchical clustering of the data acquired without ACA still yields to the formation of 7 groups with one of them being enriched with compounds belonging to clusters E, G, and J (Sup. Fig. 4). In sharp contrast, hierarchical clustering of the data acquired without our BRET probes does not allow us to identify compounds belonging to clusters E, G, and J as part of a separate group (Sup. Fig. 4). This observation points to a predominant detection of CaM inhibitors as inhibitors of TRPV1 activation by CAPS using our BRET probes.

Analysis of hit compounds not displaying CaM inhibitor activities.

Downloaded from molpharm.aspetjournals.org at ASPET Journals on March 20, 2024

Molecular Pharmacology Fast Forward. Published on June 14, 2021 as DOI: 10.1124/molpharm.121.000271
This article has not been copyedited and formatted. The final version may differ from this version.

Bibliographic pieces of evidence also support an apparent CaM-independent modulation of TRP ion channels, sometimes including TRPV1 itself, by several compounds identified as hits in our screens.

Four compounds, for which no CaM antagonist activity has been described, were identified by more than one technique to inhibit TRPV1(CAPS): (antimycin A (#17), Lovastatin (#31), Simvastatin (#47), and Sertraline (#51)) (Sup. Table 3 and Fig. 8). In the cluster F, Sertraline (#51), a 1,2,3,4-tetrahydronaphtalen derivative, which is substituted by a methylamino at position 1 and a 3,4-dichlorophenyl at position 4 (the S, S diastereoisomer), has been detected as an inhibitor by the BRET intramolecular probe and APC at +100 mV and –100 mV. Interestingly tetraline urea derivatives have been shown to display antagonistic properties against TRPV1 activation by CAPS (Messeguer *et al.*, 2006; Jetter *et al.*, 2007). While Sertraline is not a tetraline urea derivative, it would be interesting to assess whether substitution of the methylamino group of Sertraline by an urea group improve Sertraline potency and/or efficacy to inhibit CAPS-mediated TRPV1 activation. Lovastatin (#31) and Simvastatin (#47) belong to cluster I, which also contains Mevastatin (#59). All these three compounds displayed a blurred profile when comparing the results obtained using activation and inhibition modes with the different read-out assays used. Cluster I is composed of statin molecules, also known as HMG-CoA reductase inhibitors, which are a class of lipid-lowering drugs reducing illness and mortality in persons who are at high risk of cardiovascular disease. They are the most common cholesterol-lowering drugs and cholesterol binding has been shown to be of importance for TRPV1 gating (Saha *et al.*, 2017), which may point towards an indirect action of these compounds on TRPV1 activity. In our study, Simvastatin (#47) was detected as an activator by both the intermolecular BRET probe and APC, and as an inhibitor by calcium and intramolecular BRET probes. Lovastatin (#31) and Mevastatin (#59) were both detected as an activator by APC but behaved both as TRPV1 activator and inhibitor using ACA. In the literature, Lovastatin (#31) and Simvastatin (#47) have been shown to trigger TRPV1-dependent Ca^{2+} influx in endothelial cells (Su *et al.*, 2014; Negri *et al.*, 2020). However, to the best of our knowledge, an effect of Mevastatin on the activity of TRP ion channels has never been reported. Finally, two studies suggest that TRPV1 contributes to Ca^{2+} influx triggered in vagal nociceptive neurons by the well-known antibiotic antimycin A (#17) which belongs to the miscellaneous cluster (Nesuashvili *et al.*, 2013; Stanford *et al.*, 2019).

In cluster E, Raloxifen (#46), detected as a TRPV1 inhibitor only by the intramolecular BRET probe (Supp Table 3 and Fig. 8), has been shown to inhibit TRPV1 activation by CAPS in the hippocampus and dorsal root ganglion of rats (Yazğan and Nazıroğlu, 2017).

Finally, several compounds not described as CaM antagonists were shown to inhibit CAPS-induced TRPV1 activation by ACA but not by either of the two BRET probes (Supp Table 3 and Fig. 8). Bibliographic evidence exists in support of the inhibitory efficacy against CAPS-induced TRPV1 activation of 6 of these compounds. In cluster A, Flufenamic acid (#16), an anthranilic acid derivative carrying an N-(trifluoromethyl)phenyl substituent, has been shown to inhibit TRPV1 activation by CAPS (Hu *et al.*, 2010; Guinamard *et al.*, 2013). In cluster C, Mefloquine (#7) which is a quinoline derivative and the antagonistic behavior of these compounds against TRPV1 has been recently discussed (Ambatkar and Khedekar, 2019). In cluster E, Homochlorcyclizine (#19) shares structural determinants with Dexbrompheniramine which has been shown to inhibit TRPV1 in HEK293 cells (Sadofsky *et al.*, 2008). In cluster F, Rosiglitazone (#57) which belongs to the thiazolidinedione class has been shown to inhibit TRP melastatin 3 ion channel (TRPM3) while activating TRP canonical 5 ion channel (TRPC5) (Majeed *et al.*, 2011). Interestingly, during the screening of the Prestwick Chemical library with the intermolecular BRET probe, the closely related compound Troglitazone enhanced TRPV1 activation by CAPS (sup Table 2). Also, Troglitazone has been recently shown to directly activate TRPV1 (Krishnan *et al.*, 2019). Still in cluster F, Hexachlorophene (#58) is a polychloroaromatic compound shown to activate KCNQ1 ion channel (Zheng et al., 2012), a molecular event known to inhibit TRPV1 (Ambrosino *et al.*, 2019). Whether KCNQ1 ion channels are expressed in HEK293T cells is not known but outward potassium currents do exist in HEK293T cells (Ponce *et al.*, 2018) leaving room for of an indirect effect of Hexachlorophene on TRPV1. In cluster S, Epiandrosterone (5α-androstan-3β-ol-17-one) (#26) is a dehydroepiandrosterone metabolite only differing by one π-bound from 5α-androsten-3β -ol-17-one, which one has been shown to antagonize CAPS-induced activation of TRPV1 (Chen *et al.*, 2004). Auranofin (#45), an oral chrysotherapeutic agent for the treatment of rheumatoid arthritis, which belongs to the miscellaneous cluster, has been shown to activate TRPA1 but not TRPV1 in transiently transfected HEK cells using calcium assay (Mannhold *et al.*, 1987). While we also found that no TRPV1

Downloaded from molpharm.aspetjournals.org at ASPET Journals on March 20, 2024

activation was detected using a calcium assay with this compound, Auranofin, nonetheless, triggered a conformational change in TRPV1 that led to an increase of the BRET measured with the intramolecular BRET probe.

Some compounds for which we found no bibliographic evidence linking them to the TRP ion channel, calcium, or calmodulin were also detected as hits by more than one technique and might be considered for further studies. Efavirenz (#27, cluster C), a noncompetitive inhibitor of HIV-1 reverse transcriptase (RT), and Beta-Escin (#37, cluster S) has been detected as TRPV1 activator by both intermolecular BRET probes, calcium, and APC but, to the best of our knowledge, no evidence links these compounds to TRP ion channels. Importantly, Beta-Escin (#37) is known as a patch-clamp perforating agent but triggered only a very small current in non-transfected cells in our experimental conditions (Sup. Table 3), thus validating it as a potential hit. Oxethazaine (#2, cluster F), a local anesthetic, has been shown to inhibit TRPV1 activation by CAPS using both ACA and intramolecular BRET probes. Finally, we found no bibliographic evidence linking several compounds detected as hits in our primary screen by only one technique. Among these compounds, Dipyridamole (#9, cluster C), Nitrofurantoin (#14, cluster F), and Repaglinide (#53, cluster F) were detected as inhibitors or activators only by ACA. Of note, Repaglinide has been shown to target neuronal calcium sensor proteins but not Calmodulin (Okada *et al.*, 2003) and its binding to TRP ion channel is not described. Pyrvinium pamoate (#52, cluster F) and Ivermectin (#13, cluster H) were respectively detected as TRPV1 activator and inhibitor by the intramolecular BRET probe. Sulfameter (#41, cluster F) was detected as a TRPV1 activator using the intermolecular BRET probe.

Altogether, the high structural diversity of these hits could be useful for structure-activated relationship studies (Tafesse *et al.*, 2014)

Exemplification of the concept of intra- and intermolecular BRET probe design for other ion channels.

The results obtained with intra- and intermolecular BRET probes prompted us to assess whether BRET-based biosensors could be derived for other ion channels. Since not all ion channels are in interaction with Calmodulin, we focused on intramolecular BRET probes targeting ion channels having both N- and C-terminus extremities into the cytoplasm.

We first assessed whether the activity of two other TRPs ion channels, TRPV4 and TRPM8, could also be measured using intramolecular BRET probes. As shown in Fig. 9, the BRET signal measured on HEK293T cells transiently expressing mNeonG-hTRPV4-nLuc (Fig.9A) and nLuc-hTRPM8-mNeonG (Fig.9B) intramolecular BRET probes was concentration-dependently increased following addition in the cell culture medium of GSK1016790A and WS12, two specific agonists of TRPV4 and TRPM8 respectively (Bödding *et al.*, 2007; Thorneloe *et al.*, 2008). The measured half-maximal responses were consistent with those reported in the literature using patch-clamp or calcium-flux measurements on cells transiently expressing TRPV4 or TRPM8 (Bödding *et al.*, 2007; Jin *et al.*, 2011). The pharmacological selectivity of the ligand-promoted BRET changes was further demonstrated by the competitive nature of the effects, as both HC060747 and M8B, two well-known competitive antagonists of TRPV4 and TRPM8 respectively, right shifted the corresponding agonist potency to higher values in both intramolecular BRET tests. Altogether, these data strongly suggest that the agonist-promoted BRET changes in TRPV4 and TRPM8 intramolecular BRET probes correspond to activation of these two ion channels in live cells, as previously shown for TRPV1 (Ruigrok *et al.*, 2017).

To go further in the exemplification of ion channel intramolecular BRET probes, we constructed mNeon-KCa2.3-nLuc (Fig. 10A), mNeon-Kir6.1-nLuc (Fig. 10D), and mNeon-TREK1-nLuc BRET (Fig. 10G) intramolecular BRET probes targeting respectively (i) KCa2.3, a small conductance calcium-activated potassium channels sharing the same 6-transmembrane domains (TM) basic architecture with Shaker-like voltage-gated potassium channels and TRP ion channels, (ii) Kir6.1, an ATP-sensitive inwardly-rectifying potassium channels, the structure of which contains two-TM domain per monomer, and iii) TREK1, a two-pore-domain background potassium channels containing two pairs of TMs per monomer, each flanking a pore domain. The functionality of KCa2.3 was assessed in two different ways. Firstly, we co-transfected mNeonG-KCa2.3-nLuc intramolecular BRET probe with TRPV1 and Calmodulin in HEK293T cells, and triggered a Ca^{2+} influx into the cell through TRPV1 pore opening using a saturating concentration of CAPS (Fig. 10B). CAPS injection induced a rapid increase of the

Downloaded from molpharm.aspetjournals.org at ASPET Journals on March 20, 2024

Molecular Pharmacology Fast Forward. Published on June 14, 2021 as DOI: 10.1124/molpharm.121.000271
This article has not been copyedited and formatted. The final version may differ from this version.

basal BRET signal until reaching a plateau. No such effect was detected when the solvent was injected alone (vehicle). Secondly, in HEK293T cells transiently expressing mNeonG-KCa2.3-nLuc intramolecular BRET probe alone, we triggered a rise in intracellular calcium by blocking calcium transport into the sarcoplasmic and endoplasmic reticula using an increasing dose of Thapsigargin (Lu *et al.*, 2014). This produced a concentration-dependent increase of the basal BRET ratio (Fig. 10C). The Kir6.1 intramolecular BRET probe was activated using Cromakalim, a potent and selective ATP-sensitive potassium channel opener (Sanguinetti *et al.*, 1988). As expected, Cromakalim induced a rapid increase of the basal BRET signal until reaching a plateau while, again, no effect was detected when the solvent was injected alone (vehicle) (Fig. 10E). Importantly, the measured potency of Cromakalim (Fig. 10F) fell in the range already described in the literature (Wilson *et al.*, 1988). Also, Repaglinide, a known inhibitor of KiR activation by Cromakalim (Gasser *et al.*, 2003), not only right-shifted Cromakalim concentration-response curve but also decreased Cromakalim efficacy and KiR6.1 basal BRET. These observations indicate that Repaglinide is not a competitive antagonist of Cromakalim as described by others (Gasser *et al.*, 2003), but rather behaves as a non-competitive unsurmountable antagonist of Cromakalin by stabilizing KiR6.1 in a distinct conformational state. Finally, TREK1 was successfully activated using increasing quantities of the chemical activator BL1249 (Pope *et al.*, 2018) (Fig. 10H). Altogether, these results confirm that intramolecular BRET biosensors can probe the conformational changes occurring during the gating of ion channels belonging to various ion channel families and not just the TRP ion channel family.

This led us to assess whether the intramolecular BRET sensor can also probe ligand-gated ion channels such as P2X purinergic receptors that have both extremities inside the cytoplasm. We, therefore, constructed the nLuc-P2X2-mNeonG intramolecular BRET probe (Fig. 11A) and transiently transfected it in HEK293T cells. The rat P2X2 ion channel was activated in the presence of increasing quantities of ATP that induced a time-dependent decrease of the basal BRET (Fig. 11B). Dose-response analysis revealed that ATP activated the nLuc-P2X2-mNeonG intramolecular BRET probe with EC_{50} fitting the known potency of ATP to activate native P2X2, as measured using conventional techniques (North and Surprenant, 2000). These results further suggest the suitability of our intramolecular BRET probe to efficiently measure the conformational changes occurring in various ion-channel during their gating.

Downloaded from molpharm.aspetjournals.org at ASPET Journals on March 20, 2024

Molecular Pharmacology Fast Forward. Published on June 14, 2021 as DOI: 10.1124/molpharm.121.000271
This article has not been copyedited and formatted. The final version may differ from this version.

Discussion

Taking advantage of our recently published intra- and intermolecular BRET probes targeting TRPV1 ion channels activation in real time and on live cells (Ruigrok *et al.*, 2017), we have (i) assessed whether such BRET biosensors can effectively be used for high throughput purposes, (ii) performed a comparative screen of the Prestwick Chemical library with both our BRET probes and ACA, followed by the analysis of the hits using APC, and (iii) exemplified the use of intramolecular BRET probe to measure other ion channel activation.

Both intra- and intermolecular BRET probes made it possible to account for the agonist or antagonist ability of different reference compounds to modulate TRPV1 activity in live HEK293T cells (Fig. 1). While the measured potencies of each agonist obtained from each of our two BRET probes are in full agreement with the data reported in the literature and with the values measured with ACA, the pIC_{50} values measured from most of the antagonists were found to be lower by 0.5-1.5 log units (Fig. 2 and Table 1). Several experimental differences between our study and the ones in the literature may explain this discrepancy, such as the technique used to measure TRPV1 activity, the pH and temperature of the assay, the amount of CAPS needed to trigger TRPV1 activation in the presence of the various antagonists, as well as the cell model used which has been shown to directly impact both efficacy and potency of TRPV1 ligands (Bianchi *et al.*, 2006). Species-specific differences in TRPV1 functionality may also matter (Abbas, 2020). The potencies measured for each reference compound using both intra- and intermolecular BRET probes were however very close to the one measured using ACA, which is often used as the primary screen for calcium ion channels.

Most studies using APC to study TRPV1, if not all, measure the outward current at non-physiological membrane potentials (between +60 and +100 mV) and might thus highlight compounds that are not relevant for a therapeutic effect. We have shown that the choice of the membrane potential to measure the chemical activation of TRPV1 not only impacts the potency of several TRPV1 agonists and antagonists, but also drastically affects the ability of many of the tested drugs to activate or inhibit TRPV1. One likely explanation for this observation is that different ternary or quaternary conformational states of TRPV1 are stabilized when the membrane potential is clamped at various values. This observation is in agreement with the allosteric model for gating of thermo-TRPs, such as TRPV1, in which voltage, temperature, and ligands are independently coupled, either positively or negatively, to channel gating (Matta and Ahern, 2007). This is of prime importance since ligand binding is expected to be intrinsically dependent on its receptor conformation state (de Boer, 2020), thereby rehabilitating non-electrophysiological methods such as our novel BRET-based assay for ion channel HTS. Both intra- and intermolecular BRET assays achieved, moreover, excellent Z'-factors, further indicating that both BRET assays are fit enough for high-throughput screening (Fig. 3).

We then aimed at comparing the effectiveness of both intra- and intermolecular BRET assays with that of HTS conventional methods (ACA and APC) to screen the Prestwick small-sized Chemical library. Primary screening using ACA, intra- and intermolecular BRET assays indicated that 59 drugs activated TRPV1 or inhibited CAPS-induced TRPV1 activation. The results were heterogeneous since 82.6% of the hits were found by only one method. No hits were found by all three methods to behave as TRPV1 activator and only 3 drugs were found by the three assays to behave as an inhibitor of TRPV1(CAPS). Of note, out of the 33 drugs found by ACA to modulate TRPV1 activity, 8 were found to both activate and inhibit TRPV1, indicating that almost a quarter of the hits found with ACA yielded ambiguous results (supplementary Fig. 6 and Table 3). In sharp contrast, no hits were detected as both activator and inhibitor of TRPV1 using either intra- or intermolecular BRET probe.

The secondary screen of the 59 identified drugs with APC highlighted important facts. Since only 14 drugs were confirmed as TRPV1 activator or inhibitor by APC, our results mean either that both BRET probes and ACA are prone to yield a lot of false positive hits or that APC measurement is prone to yield a lot of false-negative hits. A careful review of the literature highlighted interesting clues pointing to a more balanced conclusion: First, as mentioned in the result section, 13 compounds over the 59 detected hits (~ 22% of the hits identified) are well-known Calmodulin antagonists, and 12 of them belongs to only three clusters (E, G, and J). Seven other compounds belonging to clusters E, G, or J, share structural similarities with known CaM antagonists (see result section for details). Over these 20 drugs, 15 were identified as TRPV1(CAPS) inhibitors by either one or both BRET probes while only 7 and 6 were respectively detected by ACA and APC (Fig. 8). Also, to the best of our knowledge, 19

Downloaded from molpharm.aspetjournals.org at ASPET Journals on March 20, 2024

Molecular Pharmacology Fast Forward. Published on June 14, 2021 as DOI: 10.1124/molpharm.121.000271
This article has not been copyedited and formatted. The final version may differ from this version.

other compounds known to be CaM antagonists were part of the Prestwick Chemical library but were not included in the lists of 59 drugs identified during the primary screening (Sup. Table 4). Re-analysis of the results obtained with these compounds revealed that the average inhibition efficacy of 8 of them was either very close to the drug efficacy cut-off fixed at 30%, or above but with no reproducibility between n1 and n2. These compounds, mostly detected with the intramolecular and intermolecular BRET assay, might be therefore false negatives that could have been included as positive hits using a data-driven analysis of the primary screen results instead of a subjective cut-off of the efficacy magnitude. Such workflow will be included in our further studies. Overall, these results indicate that most of the CaM antagonists included in the Prestwick Chemical library were detected as inhibitor of TRPV1 activation by CAPS. Interestingly, while Calmodulin is classically viewed as a negative modulator of TRPV1, regulating its desensitization (Numazaki et al., 2003; Rosenbaum et al., 2004; Lishko et al., 2007; Lau et al., 2012), CaM inhibition using various chemical compounds, including chlorpromazine (#3) and fluphenazine (#23), has already been shown to inhibit CAPS-induced TRPV1 activation with a potency in the µM range (Oláh et al., 2007). Whether CaM antagonists can inhibit TRPV1 through direct interaction with TRPV1 itself, by preventing the physical interaction between TRPV1 and CaM, or by another means, remains to be determined. In the light of our BRET-based repurposing drug screening results, and in the quest for new TRPV1 inhibitors, considering the CaM-TRPV1 physical and/or functional interaction as druggable is a tempting hypothesis that deserves further attention.

We also found bibliographic evidences indicating that 12 drugs out of the 59 identified during the primary screen activated or inhibited TRPV1 or other TRP ion channels without any known relation with Calmodulin. Five of these drugs were detected using either one or both BRET probes, 5 were detected using APC and 9 were detected using ACA, and no drug was detected by all three methods together. In sharp contrast with the drugs targeting CaM, which all but one belonged to only three clusters, these 12 drugs belong to various clusters without any clear relationship with their structure (see results for details and Sup. Table 3). Except for Rosiglitazone (#57) and Mefloquine (#07), no clear relationship between the chemical structure of these drugs and the prototypical structure of TRPV1 antagonists was found (Szallasi *et al.*, 2007; Ambatkar and Khedekar, 2019), suggesting an indirect role of these drugs. Interestingly, while most CaM antagonists belong to the data-driven group 7 that is mainly detected using the BRET assays, 8 of the 12 aforementioned drugs belong to group 5 which is mainly identified based on ACA data (Fig. 8). No single technique detected all hits in a single HTS run. Our study, therefore, highlights the need for benefiting from the output of different HTS platforms coupled to a multiparametric analysis to optimize future ion-channel drug-screening processes. In conclusion, based on a thorough bibliographic analysis of our results, both BRET probes (i) have proven to be as reliable as ACA or APC in identifying potential hits, (ii) provide a very specific read-out of ion channel activity, and (iii) brought back to light the CaM-TRPV1 protein-protein interaction as a druggable target for TRPV1 inhibition. Since BRET biosensors are easy to use with a low cost of implementation and have shown their adaptability to various TRPs and non-TRPs ion channels (Fig. 9-11), they may advantageously be included in ion channel drug screening campaigns.

Downloaded from molpharm.aspetjournals.org at ASPET Journals on March 20, 2024

Acknowledgments

We thank Bernard Veyret for his wise advice and proofreading of the manuscript.

Authorship Contributions.

Participated in research design: Franchet, Percherancier.

Conducted experiments: Chappe, Michel, Joushomme, Barbeau, Pierredon, Baron, Garenne, Poulletier de Gannes, Hurtier.

Performed data analysis: Chappe, Michel, Barbeau, Garenne, Pierredon, Mayer, Lagroye, Quignard, Ducret, Compan, Franchet and Percherancier.

Wrote or contributed to the writing of the manuscript: Chappe, Michel, Quignard, Lagroye, Ducret, Compan, Franchet, Percherancier.

Downloaded from molpharm.aspetjournals.org at ASPET Journals on March 20, 2024

References

Abbas MA (2020) Modulation of TRPV1 channel function by natural products in the treatment of pain. *Chemico-Biological Interactions* **330**:109178.

Abello JM, Pardalos PM, and Resende MGC (eds) (2002) *Handbook of massive data sets*, Kluwer Academic, Dordrecht ; London.

Ambatkar MP, and Khedekar PB (2019) Quinoline as TRPV1 Antagonists: A New Approach against Inflammation. *J Drug Delivery Ther* **9**:782–788.

Ambrosino P, Soldovieri MV, Di Zazzo E, Paventi G, Iannotti FA, Mosca I, Miceli F, Franco C, Canzoniero LMT, and Taglialatela M (2019) Activation of Kv7 Potassium Channels Inhibits Intracellular Ca2+ Increases Triggered By TRPV1-Mediated Pain-Inducing Stimuli in F11 Immortalized Sensory Neurons. *IJMS* **20**:4322.

Ayoub MA (2016) Resonance Energy Transfer-Based Approaches to Study GPCRs. *Methods Cell Biol* **132**:255–92, United States.

Bacart J, Corbel C, Jockers R, Bach S, and Couturier C (2008) The BRET technology and its application to screening assays. *Biotechnol J* **3**:311–324.

Bagal SK, Marron BE, Owen RM, Storer RI, and Swain NA (2015) Voltage gated sodium channels as drug discovery targets. *Channels* **9**:360–366.

Bianchi BR, Lee C-H, Jarvis MF, El Kouhen R, Moreland RB, Faltynek CR, and Puttfarcken PS (2006) Modulation of human TRPV1 receptor activity by extracellular protons and host cell expression system. *European Journal of Pharmacology* **537**:20–30.

Bödding M, Wissenbach U, and Flockerzi V (2007) Characterisation of TRPM8 as a pharmacophore receptor. *Cell Calcium* **42**:618–28, Experimentelle und Klinische Pharmakologie und Toxikologie, Universität des Saarlandes, D-66421 Homburg, Germany. matthias.boedding\@uniklinik-saarland.de, Netherlands.

Breitholtz M, Ivanov P, Ek K, and Gorokhova E (2020) Calmodulin inhibition as a mode of action of antifungal imidazole pharmaceuticals in non-target organisms. *Toxicology Research* **9**:425–430.

B.T. Priest, A.M. Swensen, and O.B. McManus (2007) Automated Electrophysiology in Drug Discovery. *CPD* **13**:2325–2337.

Butelman ER, Harris TJ, and Kreek MJ (2004) Antiallodynic Effects of Loperamide and Fentanyl against Topical Capsaicin-Induced Allodynia in Unanesthetized Primates. *J Pharmacol Exp Ther* **311**:155–163.

Butts A, DiDone L, Koselny K, Baxter BK, Chabrier-Rosello Y, Wellington M, and Krysan DJ (2013) A Repurposing Approach Identifies Off-Patent Drugs with Fungicidal Cryptococcal Activity, a Common Structural Chemotype, and Pharmacological Properties Relevant to the Treatment of Cryptococcosis. *Eukaryotic Cell* **12**:278–287.

Caldirola P, Mannhold R, and Timmerman H (1992) Overview: Calmodulin and Calmodulin-Antagonists. *Current Opinion on Therapeutic Patents* **2**:1889–1917.

Caterina MJ, Schumacher MA, Tominaga M, Rosen TA, Levine JD, and Julius D (1997) The capsaicin receptor: a heat-activated ion channel in the pain pathway. *Nature* **389**:816–24, ENGLAND.

Chandra KS, and Ramesh G (2013) The fourth-generation Calcium channel blocker: Cilnidipine. *Indian Heart Journal* **65**:691–695.

Charrad M, Ghazzali N, Boiteau V, and Niknafs A (2014) NbClust: An R Package for Determining the Relevant Number of Clusters in a Data Set. *Journal of Statistical Software* **61**:1–36.

Chen S-C, Chang T-J, and Wu F-S (2004) Competitive Inhibition of the Capsaicin Receptor-Mediated Current by Dehydroepiandrosterone in Rat Dorsal Root Ganglion Neurons. *J Pharmacol Exp Ther* **311**:529–536.

Downloaded from molpharm.aspetjournals.org at ASPET Journals on March 20, 2024

Clare JJ (2010) Targeting ion channels for drug discovery. *Discov Med* **9**:253–260.

de Boer M (2020) *The relation between intrinsic protein conformational changes and ligand binding*, Biophysics.

De-la-Rosa V, Rangel-Yescas GE, Ladrón-de-Guevara E, Rosenbaum T, and Islas LD (2013) Coarse Architecture of the Transient Receptor Potential Vanilloid 1 (TRPV1) Ion Channel Determined by Fluorescence Resonance Energy Transfer. *J Biol Chem* **288**:29506–29517.

Gasser R, Köppel H, Moosbrugger B, Esche G, Salzer M, Gasser S, and Holzmann S (2003) Indiscriminative Effects of Repaglinide and Other Specific Modulators of Transmembrane KATP-Channel Gating Properties upon Ischaemic/Hypoxic Bovine Coronary Artery Smooth Muscle Relaxation. *Journal of Clinical and Basic Cardiology* **6**:81–85.

Gavva Narender R., Bannon AW, Hovland DN, Lehto SG, Klionsky L, Surapaneni S, Immke DC, Henley C, Arik L, Bak A, Davis J, Ernst N, Hever G, Kuang R, Shi L, Tamir R, Wang J, Wang W, Zajic G, Zhu D, Norman MH, Louis J-C, Magal E, and Treanor JJS (2007) Repeated Administration of Vanilloid Receptor TRPV1 Antagonists Attenuates Hyperthermia Elicited by TRPV1 Blockade. *J Pharmacol Exp Ther* **323**:128–137.

Gavva N. R., Bannon AW, Surapaneni S, Hovland DN, Lehto SG, Gore A, Juan T, Deng H, Han B, Klionsky L, Kuang R, Le A, Tamir R, Wang J, Youngblood B, Zhu D, Norman MH, Magal E, Treanor JJS, and Louis J-C (2007) The Vanilloid Receptor TRPV1 Is Tonically Activated In Vivo and Involved in Body Temperature Regulation. *Journal of Neuroscience* **27**:3366–3374.

Gavva NR, Tamir R, Qu Y, Klionsky L, Zhang TJ, Immke D, Wang J, Zhu D, Vanderah TW, Porreca F, Doherty EM, Norman MH, Wild KD, Bannon AW, Louis J-C, and Treanor JJS (2005) Gavva 2005 J Pharmacol Exp Ther -AMG 9810 [(iE-i)-3-(4- it-i -Butylphenyl)-iN-i -(2,3-dihydrobenzo[ib-i][1,4].pdf. *J Pharmacol Exp Ther* **313**:474–484.

Global data (2020) GlobalData's Pharma Intelligence Center Drug Sales and Forecast Database.

Guinamard R, Simard C, and Del Negro C (2013) Flufenamic acid as an ion channel modulator. *Pharmacology & Therapeutics* **138**:272–284.

Gunthorpe MJ, Rami HK, Jerman JC, Smart D, Gill CH, Soffin EM, Luis Hannan S, Lappin SC, Egerton J, Smith GD, Worby A, Howett L, Owen D, Nasir S, Davies CH, Thompson M, Wyman PA, Randall AD, and Davis JB (2004) Identification and characterisation of SB-366791, a potent and selective vanilloid receptor (VR1/TRPV1) antagonist. *Neuropharmacology* **46**:133–149.

Hamdan FF, Percherancier Y, Breton B, and Bouvier M (2006) Monitoring protein-protein interactions in living cells by bioluminescence resonance energy transfer (BRET). *Curr Protoc Neurosci* **Chapter 5**:Unit 5.23, University of Montreal, Montreal, Quebec, Canada., United States.

Hasan R, Leeson-Payne ATS, Jaggar JH, and Zhang X (2017) Calmodulin is responsible for Ca2+-dependent regulation of TRPA1 Channels. *Sci Rep* **7**:45098.

Hatano N, Suzuki H, Muraki Y, and Muraki K (2013) Stimulation of human TRPA1 channels by clinical concentrations of the antirheumatic drug auranofin. *American Journal of Physiology-Cell Physiology* **304**:C354–C361.

Hegemann L, Toso SM, Lahijani KI, Webster GF, and Uitto J (1993) Direct interaction of antifungal azole-derivatives with calmodulin: a possible mechanism for their therapeutic activity. *J Invest Dermatol* **100**:343–346, United States.

Hu H, Tian J, Zhu Y, Wang C, Xiao R, Herz JM, Wood JD, and Zhu MX (2010) Activation of TRPA1 channels by fenamate nonsteroidal anti-inflammatory drugs. *Pflugers Arch - Eur J Physiol* **459**:579–592.

Hugh Reynolds C, and Claxton PTJ (1982) Inhibition of calmodulin-activated cyclic

Downloaded from molpharm.aspetjournals.org at ASPET Journals on March 20, 2024

nucleotide phosphodiesterase: Multiple binding-sites for tricyclic drugs on calmodulin. *Biochemical Pharmacology* **31**:419–421.

Jetter MC, Youngman MA, McNally JJ, McDonnell ME, Zhang S-P, Dubin AE, Nasser N, Codd EE, Flores CM, and Dax SL (2007) Heteroaryl beta-tetralin ureas as novel antagonists of human TRPV1. *Bioorg Med Chem Lett* **17**:6160–6163.

Jin M, Wu Z, Chen L, Jaimes J, Collins D, Walters ET, and O'Neil RG (2011) Determinants of TRPV4 Activity following Selective Activation by Small Molecule Agonist GSK1016790A. *PLoS ONE* **6**:e16713.

Johnson JD, and Wittenauer LA (1983) A fluorescent calmodulin that reports the binding of hydrophobic inhibitory ligands. *Biochemical Journal* **211**:473–479.

Kaczorowski GJ, McManus OB, Priest BT, and Garcia ML (2008) Ion Channels as Drug Targets: The Next GPCRs. *Journal of General Physiology* **131**:399–405.

Kassambara A, and Mundt F (2020) *factoextra: Extract and Visualize the Results of Multivariate Data Analyses*.

Kirkton RD, and Bursac N (2011) Engineering biosynthetic excitable tissues from unexcitable cells for electrophysiological and cell therapy studies. *Nat Commun* **2**:300.

Kocan M, and Pfleger KDG (2011) Study of GPCR-protein interactions by BRET. *Methods Mol Biol* **746**:357–71, United States.

Krishnan V, Baskaran P, and Thyagarajan B (2019) Troglitazone activates TRPV1 and causes deacetylation of PPARγ in 3T3-L1 cells. *Biochim Biophys Acta Mol Basis Dis* **1865**:445–453.

Lau S-YY, Procko E, and Gaudet R (2012) Distinct properties of Ca2+-calmodulin binding to N- and C-terminal regulatory regions of the TRPV1 channel. *J Gen Physiol* **140**:541–55, United States.

Lishko PV, Procko E, Jin X, Phelps CB, and Gaudet R (2007) The Ankyrin Repeats of TRPV1 Bind Multiple Ligands and Modulate Channel Sensitivity. *Neuron* **54**:905–918.

Lu Y-C, Yang J, Ding G-L, Shi S, Zhang D, Jin L, Pan J-X, Lin X-H, Zhu Y-M, Sheng J-Z, and Huang H-F (2014) Small-Conductance, Calcium-Activated Potassium Channel 3 (SK3) Is a Modulator of Endometrial Remodeling During Endometrial Growth. *The Journal of Clinical Endocrinology & Metabolism* **99**:3800–3810.

Lübker C, and Seifert R (2015) Effects of 39 Compounds on Calmodulin-Regulated Adenylyl Cyclases AC1 and Bacillus anthracis Edema Factor. *PLoS ONE* **10**:e0124017.

Majeed Y, Bahnasi Y, Seymour VAL, Wilson LA, Milligan CJ, Agarwal AK, Sukumar P, Naylor J, and Beech DJ (2011) Rapid and Contrasting Effects of Rosiglitazone on Transient Receptor Potential TRPM3 and TRPC5 Channels. *Mol Pharmacol* **79**:1023–1030.

Mannhold R, Kramer A, Schäfer W, and Schramm P (1987) CaM-Inhibitory Actions of Ca Antagonists. *Arch Pharm Pharm Med Chem* **320**:683–692.

Matta JA, and Ahern GP (2007) Voltage is a partial activator of rat thermosensitive TRP channels. *The Journal of physiology* **585**:469–482, Wiley Online Library.

McGivern JG, and Ding M (2020) Ion Channels and Relevant Drug Screening Approaches. *SLAS DISCOVERY: Advancing the Science of Drug Discovery* **25**:413–419.

Merritt J, BROWN B, and TOMLINSON S (1982) LOPERAMIDE AND CALMODULIN. *The Lancet* **319**:283.

Meseguer V, Karashima Y, Talavera K, D'Hoedt D, Donovan-Rodriguez T, Viana F, Nilius B, and Voets T (2008) Transient Receptor Potential Channels in Sensory Neurons Are Targets of the Antimycotic Agent Clotrimazole. *Journal of Neuroscience* **28**:576–586.

Messeguer A, Planells-Cases R, and Ferrer-Montiel A (2006) Physiology and Pharmacology of the Vanilloid Receptor. *CN* **4**:1–15.

Micheli D, Collodel A, Semeraro C, Gaviraghi G, and Carpi C (1990) Lacidipine: a calcium antagonist with potent and long-lasting antihypertensive effects in animal studies. *J*

Downloaded from molpharm.aspetjournals.org at ASPET Journals on March 20, 2024

Cardiovasc Pharmacol **15**:666–675.

Miyawaki A, and Niino Y (2015) Molecular spies for bioimaging–fluorescent protein-based probes. *Molecular cell* **58**:632–43, Laboratory for Cell Function Dynamics, Brain Science Institute, RIKEN, 2-1 Hirosawa,.

Montero M, Alvarez J, and Garcia-Sancho J (1991) Agonist-induced Ca2+ influx in human neutrophils is secondary to the emptying of intracellular calcium stores. *Biochemical Journal* **277**:73–79.

Negri S, Faris P, Rosti V, Antognazza MR, Lodola F, and Moccia F (2020) Endothelial TRPV1 as an Emerging Molecular Target to Promote Therapeutic Angiogenesis. *Cells* **9**:1341.

Nesuashvili L, Hadley SH, Bahia PK, and Taylor-Clark TE (2013) Sensory nerve terminal mitochondrial dysfunction activates airway sensory nerves via transient receptor potential (TRP) channels. *Mol Pharmacol* **83**:1007–1019.

Norman JA, Ansell J, Stone GA, Wennogle LP, and Wasley JW (1987) CGS 9343B, a novel, potent, and selective inhibitor of calmodulin activity. *Mol Pharmacol* **31**:535–540, United States.

North RA, and Surprenant A (2000) Pharmacology of Cloned P2X Receptors. *Annu Rev Pharmacol Toxicol* **40**:563–580.

Numazaki M, Tominaga T, Takeuchi K, Murayama N, Toyooka H, and Tominaga M (2003) Structural determinant of TRPV1 desensitization interacts with calmodulin. *Proc Natl Acad Sci U S A* **100**:8002–6, United States.

Obergrussberger A, Goetze TA, Brinkwirth N, Becker N, Friis S, Rapedius M, Haarmann C, Rinke-Weiß I, Stölzle-Feix S, Brüggemann A, George M, and Fertig N (2018) An update on the advancing high-throughput screening techniques for patch clamp-based ion channel screens: implications for drug discovery. *Expert Opinion on Drug Discovery* **13**:269–277.

Okada M, Takezawa D, Tachibanaki S, Kawamura S, Tokumitsu H, and Kobayashi R (2003) Neuronal calcium sensor proteins are direct targets of the insulinotropic agent repaglinide. *Biochemical Journal* **375**:87–97.

Oláh Z, Jósvay K, Pecze L, Letoha T, Babai N, Budai D, Ötvös F, Szalma S, and Vizler C (2007) Anti-calmodulins and Tricyclic Adjuvants in Pain Therapy Block the TRPV1 Channel. *PLoS ONE* **2**:e545.

Papakosta M, Dalle C, Haythornthwaite A, Cao L, Stevens EB, Burgess G, Russell R, Cox PJ, Phillips SC, and Grimm C (2011) The Chimeric Approach Reveals That Differences in the TRPV1 Pore Domain Determine Species-specific Sensitivity to Block of Heat Activation. *J Biol Chem* **286**:39663–39672.

Percherancier Y, Germain-Desprez D, Galisson F, Mascle XH, Dianoux L, Estephan P, Chelbi-Alix MK, and Aubry M (2009) Role of SUMO in RNF4-mediated promyelocytic leukemia protein (PML) degradation: sumoylation of PML and phospho-switch control of its SUMO binding domain dissected in living cells. *J Biol Chem* **284**:16595–608, CNRS FRE2937, Institut André Lwoff, Villejuif 94801, France., United States.

Pfleger KDG, Seeber RM, and Eidne KA (2006) Bioluminescence resonance energy transfer (BRET) for the real-time detection of protein-protein interactions. *Nat Protoc* **1**:337–45, England.

Ponce A, Castillo A, Hinojosa L, Martinez-Rendon J, and Cereijido M (2018) The expression of endogenous voltage-gated potassium channels in HEK293 cells is affected by culture conditions. *Physiol Rep* **6**:e13663.

Pope L, Arrigoni C, Lou H, Bryant C, Gallardo-Godoy A, Renslo AR, and Minor DL (2018) Protein and Chemical Determinants of BL-1249 Action and Selectivity for K_{2P} Channels. *ACS Chem Neurosci* **9**:3153–3165.

Premkumar LS, Agarwal S, and Steffen D (2002) Single-channel properties of native and

Downloaded from molpharm.aspetjournals.org at ASPET Journals on March 20, 2024

cloned rat vanilloid receptors. *The Journal of Physiology* **545**:107–117.

Prozialeck WC, and Weiss B (1982) Inhibition of calmodulin by phenothiazines and related drugs: structure-activity relationships. *Journal of Pharmacology and Experimental Therapeutics* **222**:509–516, American Society for Pharmacology and Experimental Therapeutics.

R Core Team (2020) *R: A Language and Environment for Statistical Computing*, R Foundation for Statistical Computing, Vienna, Austria.

Ralevic V, Kendall DA, Jerman JC, Middlemiss DN, and Smart D (2001) Cannabinoid activation of recombinant and endogenous vanilloid receptors. *European Journal of Pharmacology* **424**:211–219.

Rani N, Sharma A, Gupta G, and Singh R (2013) Imidazoles as Potential Antifungal Agents: A Review. *MRMC* **13**:1626–1655.

Robertson DN, Sleno R, Nagi K, Pétrin D, Hébert TE, and Pineyro G (2016) Design and construction of conformational biosensors to monitor ion channel activation: A prototype FlAsH/BRET-approach to Kir3 channels. *Methods* **92**:19–35.

Rochette-Egly C, Boschetti E, Basset P, and Egly JM (1982) Interactions between calmodulin and immobilized phenothiazines. *J Chromatogr* **241**:333–344, Netherlands.

Rosenbaum T, Gordon-Shaag A, Munari M, and Gordon SE (2004) Ca2+/calmodulin modulates TRPV1 activation by capsaicin. *J Gen Physiol* **123**:53–62, United States.

Ruigrok HJ, Shahid G, Goudeau B, Poulletier de Gannes F, Poque-Haro E, Hurtier A, Lagroye I, Vacher P, Arbault S, Sojic N, Veyret B, and Percherancier Y (2017) Full-Spectral Multiplexing of Bioluminescence Resonance Energy Transfer in Three TRPV Channels. *Biophys J* **112**:87–98, United States.

Sadofsky LR, Campi B, Trevisani M, Compton SJ, and Morice AH (2008) Sadofsky 2008 Experimental Lung Research -TRANSIENT RECEPTOR POTENTIAL VANILLOID-1–MEDIATED CALCIUM RESPONSES ARE INHIBITED BY THE ALKYLAMINE ANTIHISTAMINES.pdf. *Experimental Lung Research* **34**:681–693.

Saha S, Ghosh A, Tiwari N, Kumar Ashutosh, Kumar Abhishek, and Goswami C (2017) Preferential selection of Arginine at the lipid-water-interface of TRPV1 during vertebrate evolution correlates with its snorkeling behaviour and cholesterol interaction. *Sci Rep* **7**:16808.

Sanguinetti MC, Scott AL, Zingaro GJ, and Siegl PK (1988) BRL 34915 (cromakalim) activates ATP-sensitive K+ current in cardiac muscle. *Proceedings of the National Academy of Sciences* **85**:8360–8364.

Schaeffer P, Luginer C, Follenius-Wund A, Gerard D, and Stoclet J-C (1987) Comparative effects of calmodulin inhibitors on calmodulin's hydrophobic sites and on the activation of cyclic nucleotide phosphodiesterase by calmodulin. *Biochemical Pharmacology* **36**:1989–1996.

Schann S, Bouvier M, and Neuville P (2013) Technology combination to address GPCR allosteric modulator drug-discovery pitfalls. *Drug Discov Today Technol* **10**:e261-7, England.

Stanford KR, Hadley SH, Barannikov I, Ajmo JM, Bahia PK, and Taylor-Clark TE (2019) Antimycin A-induced mitochondrial dysfunction activates vagal sensory neurons via ROS-dependent activation of TRPA1 and ROS-independent activation of TRPV1. *Brain Research* **1715**:94–105.

Su K-H, Lin S-J, Wei J, Lee K-I, Zhao J-F, Shyue S-K, and Lee T-S (2014) The essential role of transient receptor potential vanilloid 1 in simvastatin-induced activation of endothelial nitric oxide synthase and angiogenesis. *Acta Physiol* **212**:191–204.

Swanson DM, Dubin AE, Shah C, Nasser N, Chang L, Dax SL, Jetter M, Breitenbucher JG, Liu C, Mazur C, Lord B, Gonzales L, Hoey K, Rizzolio M, Bogenstaetter M, Codd EE, Lee DH, Zhang S-P, Chaplan SR, and Carruthers NI (2005) Identification and Biological

Downloaded from molpharm.aspetjournals.org at ASPET Journals on March 20, 2024

Evaluation of 4-(3-Trifluoromethylpyridin-2-yl)piperazine-1-carboxylic Acid (5-Trifluoromethylpyridin-2-yl)amide, a High Affinity TRPV1 (VR1) Vanilloid Receptor Antagonist. *J Med Chem* **48**:1857–1872.

Szallasi A, Cortright DN, Blum CA, and Eid SR (2007) The vanilloid receptor TRPV1: 10 years from channel cloning to antagonist proof-of-concept. *Nat Rev Drug Discov* **6**:357–72, England.

Tafesse L, Kanemasa T, Kurose N, Yu J, Asaki T, Wu G, Iwamoto Y, Yamaguchi Y, Ni C, Engel J, Tsuno N, Patel A, Zhou X, Shintani T, Brown K, Hasegawa T, Shet M, Iso Y, Kato A, and Kyle DJ (2014) Structure–Activity Relationship Studies and Discovery of a Potent Transient Receptor Potential Vanilloid (TRPV1) Antagonist 4-[3-Chloro-5-[(1 *S*)-1,2-dihydroxyethyl]-2-pyridyl]- *N* -[5-(trifluoromethyl)-2-pyridyl]-3,6-dihydro-2 *H* -pyridine-1-carboxamide (V116517) as a Clinical Candidate for Pain Management. *J Med Chem* **57**:6781–6794.

Terstappen GC, Roncarati R, Dunlop J, and Peri R (2010) Screening technologies for ion channel drug discovery. *Future Med Chem* **2**:715–30, England.

Thorneloe KS, Sulpizio AC, Lin Z, Figueroa DJ, Clouse AK, McCafferty GP, Chendrimada TP, Lashinger ES, Gordon E, and Evans L (2008) N-((1S)-1-[4-((2S)-2-{[(2, 4-dichlorophenyl) sulfonyl] amino}-3-hydroxypropanoyl)-1-piperazinyl] carbonyl}-3-methylbutyl)-1-benzothiophene-2-carboxamide (GSK1016790A), a novel and potent transient receptor potential vanilloid 4 channel agonist induces urinary bladder contraction and hyperactivity: Part I. *Journal of Pharmacology and Experimental Therapeutics* **326**:432–442, ASPET.

Tominaga M, Caterina MJ, Malmberg AB, Rosen TA, Gilbert H, Skinner K, Raumann BE, Basbaum AI, and Julius D (1998) The Cloned Capsaicin Receptor Integrates Multiple Pain-Producing Stimuli. *Neuron* **21**:531–543.

Volpi M, Sha'afi RI, Epstein PM, Andrenyak DM, and Feinstein MB (1981) Local anesthetics, mepacrine, and propranolol are antagonists of calmodulin. *Proceedings of the National Academy of Sciences* **78**:795–799.

Wickenden A, Priest B, and Erdemli G (2012) Ion channel drug discovery: challenges and future directions. *Future Medicinal Chemistry* **4**:661–679.

Wickham H (2016) *ggplot2: Elegant Graphics for Data Analysis*, Springer-Verlag New York.

Wickham H, François R, Henry L, and Müller K (2020) *dplyr: A Grammar of Data Manipulation*.

Wilson C, Coldwell MC, Howlett DR, Cooper SM, and Hamilton TC (1988) Comparative effects of K+ channel blockade on the vasorelaxant activity of cromakalim, pinacidil and nicorandil. *European Journal of Pharmacology* **152**:331–339.

Winter J, Dray A, Wood JN, Yeats JC, and Bevan S (1990) Cellular mechanism of action of resiniferatoxin: a potent sensory neuron excitotoxin. *Brain Research* **520**:131–140.

Xin HB, and Zhang BH (1993) [Inhibitory effects of cyproheptadine on calmodulin activated Ca(2+)-ATPase activity of rabbit erythrocyte membranes]. *Zhongguo Yao Li Xue Bao* **14 Suppl**:S5-7, China.

Yazğan Y, and Nazıroğlu M (2017) Ovariectomy-Induced Mitochondrial Oxidative Stress, Apoptosis, and Calcium Ion Influx Through TRPA1, TRPM2, and TRPV1 Are Prevented by 17β-Estradiol, Tamoxifen, and Raloxifene in the Hippocampus and Dorsal Root Ganglion of Rats. *Mol Neurobiol* **54**:7620–7638.

Yu H, Li M, Wang W, and Wang X (2016) High throughput screening technologies for ion channels. *Acta Pharmacol Sin* **37**:34–43.

Zhang JH, Chung TD, and Oldenburg KR (1999) A Simple Statistical Parameter for Use in Evaluation and Validation of High Throughput Screening Assays. *J Biomol Screen* **4**:67–

Downloaded from molpharm.aspetjournals.org at ASPET Journals on March 20, 2024

Molecular Pharmacology Fast Forward. Published on June 14, 2021 as DOI: 10.1124/molpharm.121.000271
This article has not been copyedited and formatted. The final version may differ from this version.

73, DuPont Pharmaceuticals Research Laboratories, Leads Discovery, DuPont Pharmaceuticals Company, Wilmington, Delaware., United States.

Downloaded from molpharm.aspetjournals.org at ASPET Journals on March 20, 2024

Footnotes.

The research leading to these results received funding from Aquitaine Science Transfert, the Technology Transfer Accelerator Office of New Aquitaine (France); the French National Research Agency (ANR) (grant agreement ANR-19-CE44-0010-02, the CANALBRET project); and the New Aquitaine regional council (grant agreement AAPR2020I-2019- 8140410, The PHYSTRIG project).

The authors declare that there is no conflict of interest.

Downloaded from molpharm.aspetjournals.org at ASPET Journals on March 20, 2024

Molecular Pharmacology Fast Forward. Published on June 14, 2021 as DOI: 10.1124/molpharm.121.000271
This article has not been copyedited and formatted. The final version may differ from this version.

Figure legends

Figure 1: Measuring TRPV1 activity using an intramolecular or an intermolecular BRET. (A) Schematic representation of the sYFP2-TRPV1-rLuc2 intramolecular BRET probe, where sYFP2 was fused to the N-terminal extremity of TRPV1 while rLuc2 was fused to the C-terminal extremity of TRPV1. Following activation of TRPV1, the distance (d) and/or the orientation (o) between rLuc2 and sYFP2 are expected to be modified during TRPV1 gating and subsequent conformational changes of TRPV1 subunits (Ruigrok *et al.*, 2017). (B) Schematic representation of the intermolecular BRET assay assessing the coupling of TRPV1 to Calmodulin. sYFP2 was fused to the N-terminal of Calmodulin and rLuc2 to the C-terminal of TRPV1. Following activation of TRPV1, TRPV1 coupling to CaM is expected to be increased thereby affecting the distance d between rLuc2 and sYFP2. (C & D) Concentration-response curves of various agonists-induced BRET changes measured in HEK293T cells expressing the sYFP2-TRPV1-rLuc2 BRET probe (C, n=5 for all compounds) or the TRPV1-rLuc2/sYFP2-CaM constructs (D, n=9 for CAPS, n=5 for RTX, n=4 for Olvanil and OLDA). (E & F) Concentration-response curves of the ability of various antagonists to inhibit CAPS (500nM) induced BRET changes in HEK293T cells expressing the sYFP2-TRPV1-rLuc2 BRET probe (E, n=4 for all compounds) or the TRPV1-rLuc2/sYFP2-CaM constructs (F, n=4 for all compounds).

Figure 2: Comparison of the reference agonist and antagonist potencies when measured in HTS conditions using either the intramolecular BRET probe, the intermolecular BRET probe, Automated Patch Clamp (APC), or Automated Calcium Assay (ACA).

Figure 3: Validation of the suitability of the intramolecular and intermolecular BRET assays targeting TRPV1 for high-throughput screening (HTS). (A & B) Assessment of the technical and biological reproducibility to measure CAPS-induced dose-dependent increase of the BRET signal measured with intramolecular (A) and intermolecular (B) BRET probes targeting TRPV1. Two sets of four independent dose responses were performed on two different days using each BRET sensor to verify that all concentration-response curves fall within three standard deviations of the mean. (C & D) Z'-factor: Cells transfected with the sYFP2-TRPV1-rLuc2 intramolecular BRET probe (C) or coexpressing TRPV1-rLuc2 and sYFP2-Calmodulin (D) were seeded in white opaque tissue culture 384 well plates (see material and methods for details). BRET measurements were performed in the presence or absence of CAPS at a concentration equivalent to the EC_{80} (500 nM). In total, 5 consecutive 384-well plates were processed over 3 consecutive days with 16-24 wells read per plate and per condition. Z'-factor were calculated using the following formula (Zhang *et al.*, 1999) : Z' =

$$1 - [3 \times SD(BRETagonist) + 3 \times SD(BRETbasal)] / [Mean(BRETagonist) - Mean(BRETbasal)],$$

where SD = standard deviation.

Figure 4: Screening of the Prestwick Chemical Library for identification of TRPV1 activators. "n1" and "n2" stand to the first and second screens. (A, B, C) Identification of candidate compounds activating TRPV1 in the primary screen of the Prestwick chemical library using the intramolecular BRET probe (A), the intermolecular BRET assay (B), and the automated calcium assay (C). The concentration of the compound tested was 15 µM in each test. Values were normalized to the maximal efficacy measured in presence of 4 µM CAPS (ACA) or 15 µM CAPS (BRET assays). Positive candidate compounds were identified by a relative efficacy of at least 30% of maximal CAPS efficacy in the two independent technical replicates of the screen (area in grey). (D, E, F) Histogram of relative compounds efficacies to induce TRPV1 activation when assessed with the intramolecular BRET probe (D), the intermolecular BRET assay (E), and automated calcium assay (F). The x-axes were bounded in the [-30, 75] interval to align the histograms horizontally. The numbers of non-displayed values are 7, 1,7, and 110 for intramolecular BRET, intermolecular BRET, and calcium assays, respectively. (G, H, I) Scatter plot of the Prestwick Chemical library screen performed in duplicate with the intramolecular BRET probe (G), the intermolecular BRET assay (H), and the automated calcium assay (I). The red line represents the y=x equation.

Downloaded from molpharm.aspetjournals.org at ASPET Journals on March 20, 2024

Figure 5: Screening of the Prestwick chemical Chemical library for identification of inhibitors of TRPV1 activation by CAPS. "n1" and "n2" stand to the first and second screens. (A, B, C) Identification of candidate compounds inhibiting TRPV1(CAPS) in the primary screen of the Prestwick Chemical library using the intramolecular BRET probe (A), the intermolecular BRET assay (B), and the automated calcium assay (C). The concentration of the compound tested was 10 µM in each test. Values were normalized to the maximal efficacy measured in presence of 500 nM CAPS (BRET assays) or 100 nM CAPS (ACA). Candidate compounds were characterized as hits if they induced a decrease of at least 30% of CAPS efficacy in the two technical replicates of the screen (area in grey). (D, E, F) Histogram of relative compounds efficacies to induce TRPV1 activation when assessed with the intramolecular BRET probe (D), the intermolecular BRET assay (E), and automated calcium assay (F). The x-axes were bounded in the [-30, 70] interval to align the histograms horizontally. The numbers of non-displayed values are 88, 5,9, and 197 for intramolecular BRET, intermolecular BRET, and calcium assays, respectively. (G, H, I) Scatter plot of the Prestwick Chemical library screen performed in duplicate with the intramolecular BRET probe (G), the intermolecular BRET assay (H), and automated calcium assay (I). The red line represents the y=x equation.

Figure 6: Venn diagram of the hits detected with the TRPV1 intramolecular BRET probe, TRPV1 intermolecular BRET assay, and ACA.

Figure 7: Influence of the imposed membrane potential on the ability of hit compounds to activate TRPV1 or inhibit TRPV1 activation by CAPS. (A) I–V curves of vehicle (blue curve) or CAPS (1 µM, red curve)-evoked currents in HEK cells stably expressing hTRPV1. (B) The concentration-response curve of CAPS (left panel, n=44) or CPZ (right panel, n=21)-evoked current measured at +100 mV, -25 mV, and -100 mV in HEK cells stably expressing hTRPV1. CPZ concentration-response curves were measured 2-3 minutes after the addition of 50 nM CAPS in the assay buffer. (C) Scatter plot of the ability of hit compounds to activate TRPV1 when the membrane potential is clamped to -25 mV vs +100 mV (left panel) or -100 mV vs +100 mV (right panel). (D) Scatter plot of the ability of hit compounds to inhibit CAPS (50 nM)-activated TRPV1 when the membrane potential is clamped to -25 mV vs +100 mV (left panel) or -100 mV vs +100 mV (right panel).

Figure 8: Data-driven hierarchical clustering of the effect of the hit compounds. The NbClust R package automatically sorted the 54 analyzed hits in 7 different groups. A complete linkage method (default method based on farthest neighbors distance) was then applied to hierarchical clustering of the hits into each group using a maximum (Chebychev) distance metric (Abello *et al.*, 2002). Correspondence with the structure-driven clustering and the measured activity of the drug as assessed with each technique in both activation and inhibition mode is also indicated. "X" indicates that the indicated drug efficacy was equal or above 30% of CAPS efficacy to trigger TRPV1 activation (activation mode) or inhibited TRPV1 activation by CAPS by at least 30% (see material and methods for details). "X*" indicates that the indicated drug did not inhibit but potentiated TRPV1 activation by CAPS (see Sup. Table 3 for quantitative analysis). Whether each compound is identified as CaM inhibitor (Cam_Inh) or putative CaM inhibitor (p_Cam_Inh) is also indicated (see results for details).

Figure 9: Assessment of the functionality of intramolecular BRET probes targeting TRPM8 and TRPV4. (A) Concentration-response curves of the TRPV4 agonist GSK1016790A measured in HEK293T cells expressing the mNeonG-TRPV4-nLuc BRET probe, either in presence of the TRPV4 antagonist HC060747 (10 µM, n=3) or an equivalent quantity of solvent (vehicle, n=3). The pEC_{50} of GSK1016790A was 7.91±0.11. (B) Concentration-response curves of the TRPM8 agonist WS12 measured in HEK293T cells expressing the nLuc-TRPM8-mNeonG BRET probe, either in presence of the TRPM8 antagonist M8B (10 µM, n=6) or an equivalent quantity of solvent (vehicle, n=4). The pEC_{50} of WS12 was 6.48±0.21. Insets: schematic representation of mNeonGreen-TRPV4-nLuc and nLuc-TRPM8-mNeonGreen intramolecular BRET probes.

Figure 10: Assessment of the functionality of intramolecular BRET probes targeting KCa2.3, KiR6.1, and TREK1. (A) Schematic representation of mNeonGreen-KCa2.3-nLuc intramolecular

Downloaded from molpharm.aspetjournals.org at ASPET Journals on March 20, 2024

Molecular Pharmacology Fast Forward. Published on June 14, 2021 as DOI: 10.1124/molpharm.121.000271
This article has not been copyedited and formatted. The final version may differ from this version.

BRET probe. (B) Kinetic measurement of the effect of CAPS (10 µM) or vehicle on the BRET ratio measured from HEK293T cells co-expressing mNeon-KCa2.3-nLuc intramolecular BRET probe, untagged TRPV1 ion channel, and CaM (n=5). The dashed line indicates the time of the injection. (C) Dose-response curves of Thapsigargin on the BRET ratio measured from HEK293T cells transfected with the mNeonG-KCa2.3-nLuc BRET probe (n=3). The pEC_{50} of Thapsigargin was 7.68±0.17. (D) Schematic representation of mNeonGreen-Kir6.1-nLuc intramolecular BRET probe. (E) Kinetic measurement of the effect of Cromakalim or vehicle on the BRET ratio measured from HEK293T cells co-expressing the mNeon-KiR6.1-nLuc and SUR1 subunits (n=3). The dashed line indicates the time of the injection. (F) Dose-response curves of the KiR6.1 agonist Cromakalim (CRK), injected in the presence or absence of Repaglinide (10 µM), on the BRET ratio measured from HEK293T cells transfected with the mNeonG-KiR6.1-nLuc BRET probe (n=4 for Vehicle and n=3 for RPG). The pEC_{50} of CRK was 7.84±0.18. (G) Schematic representation of mNeonGreen-TREK1-nLuc intramolecular BRET probe. (H) Kinetic measurement of the effect of increasing dose of BL1249 or vehicle on the BRET ratio measured from HEK293T cells co-expressing the mNeon-TREK1-nLuc intramolecular BRET probe (n=3).

Figure 11: (A) Schematic representation of the nLuc-P2X2-mNeonGreen intramolecular BRET probe, where nLuc was fused to the N-terminal extremity of rat P2X2 while mNeonGreen was fused to the C-terminal extremity. Following activation of P2X2, the distance (d) and/or the orientation (o) between nLuc and mNeonGreen are expected to be modified during P2X2 gating and subsequent conformational changes of P2X2 subunits. (B) Kinetic measurement of the effect of increasing dose of ATP on the BRET ratio measured from HEK293T cells expressing the nLuc-P2X2-mNeonGreen intramolecular BRET probe (n=3). (C) Concentration-response curves of ATP on the BRET ratio measured from HEK293T cells transfected with the nLuc-P2X2-mNeonGreen BRET biosensor (n=3). The pEC50 of ATP was 4,99±0,305

Downloaded from molpharm.aspetjournals.org at ASPET Journals on March 20, 2024

Molecular Pharmacology Fast Forward. Published on June 14, 2021 as DOI: 10.1124/molpharm.121.000271
This article has not been copyedited and formatted. The final version may differ from this version.

Tables

Table 1: List of characteristics used for data-driven hierarchical clustering

Activation mode (% of CAPS effect)						Inhibition mode (% of inhibition)					
Bret intra	Bret inter	Calcium	APC 100 mV	APC 25 mV	APC –100 mV	Bret intra	Bret inter	Calcium	APC 100 mV	APC –25 mV	APC –100 mV

Downloaded from molpharm.aspetjournals.org at ASPET Journals on March 20, 2024

Table 2: pEC_{50} / pIC_{50} values derived from curve fitting of TRPV1 agonists/antagonists dose-response measured using YFP-TRPV1-Luc intramolecular BRET probe, TRPV1-Luc/YFP-CaM intermolecular BRET probe, automated-Ca2+ flux assay (ACA), and automated-patch clamp assay (APC). BRET assays were measured both in 96-well plate and 384 well plate's formats. Values represent the means ± S.E. of 3-9 independent experiments performed in duplicate. Values found in the literature are also indicated along with the method used, cellular model, and reference.

	Compound	Intramolecular BRET probe		Intermolecular BRET probe		ACA	APC	Potency found in the literature	method	Cellular model	reference
		96 wells	384 wells	96 wells	384 wells						
Agonists	**Capsaïcin**	6.96±0.07	6.83±0.05	6.73±0.10	7.11±0.21	8.05±0.08	7.45±0.03	7.1 - 7.3	Ca^{2+}(Fluo3/4)	HEK293	(Ralevic *et al.*, 2001; Bianchi *et al.*, 2006)
Agonists	**Olvanil**	5.89±0.10	6.95±0.05	6.42±0.11	8.42±0.16	7.93±0.13	7.59±0.04	6.36 - 7.73	Ca^{2+}(Fluo3/4)	HEK293	(Ralevic *et al.*, 2001; Bianchi *et al.*, 2006)
Agonists	**OLDA**	6.96±0.74	4.94±0.11	4.90±0.31	5.99±0.30	6.20±0.10	5.64±0.05	5.49±0.06	Ca^{2+}(Fluo4)	HEK293	(Bianchi *et al.*, 2006)
Agonists	**RTX**	8.02±0.08	8.34±0.06	7.59±0.08	8.12±0.18	8.19±0.08	8.24±0.04	7.92 – 8.69	^{45}Ca uptake Ca^{2+}(Fluo4)	HEK293 neurons	(Winter *et al.*, 1990; Bianchi *et al.*, 2006)
Antagonists	**AMG 517**	7.12±0.10	7.95±0.14	6.97±0.07	7.87±0.05	8.12±0.09	8.40±0,05	9.19±0,25	^{45}Ca uptake	CHO	(Narender R. Gavva *et al.*, 2007)
Antagonists	**JNJ17203212**	6.12±0.11	6.91±0.07	6.34±0.06	6.47±0.09	6.96±0.02	8.24±0,06	7.20±0.11	Ca^{2+}(Fluo3)	HEK293	(Swanson *et al.*, 2005)
Antagonists	**BCTC**	8.05±0.14	7.55±0.05	7.54±0.10	7.30±0.02	8.02±0.01	9.06±0.02	8.77±0.01	Calcium4	CHO-Trex	(Papakosta *et al.*, 2011)
Antagonists	**SB 366791**	6.15±0.35	6.47±0.14	5.83±0.21	6.45±0.20	5.58±0.08	7.84±0.06	6.89±0.22	^{45}Ca uptake	CHO	(Gunthorpe *et al.*, 2004; Gavva *et al.*, 2005)
Antagonists	**AMG 9810**	6.12±0.10	6.51±0.32	6.55±0.06	6.45±0.09	6.31±0.05	8.12±0.04	7.72±0.33	^{45}Ca uptake	CHO	(Gavva *et al.*, 2005)
Antagonists	**AMG 21629**	7.8±0.18	8.64±0.06	7.84±0.09	8.35±0.06	8.42±0.04	8.64±0.08	9.28±0.23	^{45}Ca uptake	CHO	(N. R. Gavva *et al.*, 2007)

Downloaded from molpharm.aspetjournals.org at ASPET Journals on March 20, 2024

	Capsazepine	6.31±0.08	n.d.	6.19±0.14	n.d.	6.32±0.04	8.40±0.06	7.90 – 8.27	^{45}Ca uptake Ca^{2+}(Fluo4)	CHO HEK	(Gavva *et al.*, 2005; Bianchi *et al.*, 2006)

Downloaded from molpharm.aspetjournals.org at ASPET Journals on March 20, 2024

Molecular Pharmacology Fast Forward. Published on June 14, 2021 as DOI: 10.1124/molpharm.121.000271
This article has not been copyedited and formatted. The final version may differ from this version.

Table 3: % of confirmed hit between replicates assays. The number of confirmed hits found for each method is indicated in parenthesis.

	Intramolecular BRET probe	Intermolecular BRET probe	Calcium assay
Agonist mode	100% (3)	87.5% (7)	18.1% (16)
Antagonist mode	42.6% (23)	58.8% (10)	31.2% (28)

Downloaded from molpharm.aspetjournals.org at ASPET Journals on March 20, 2024

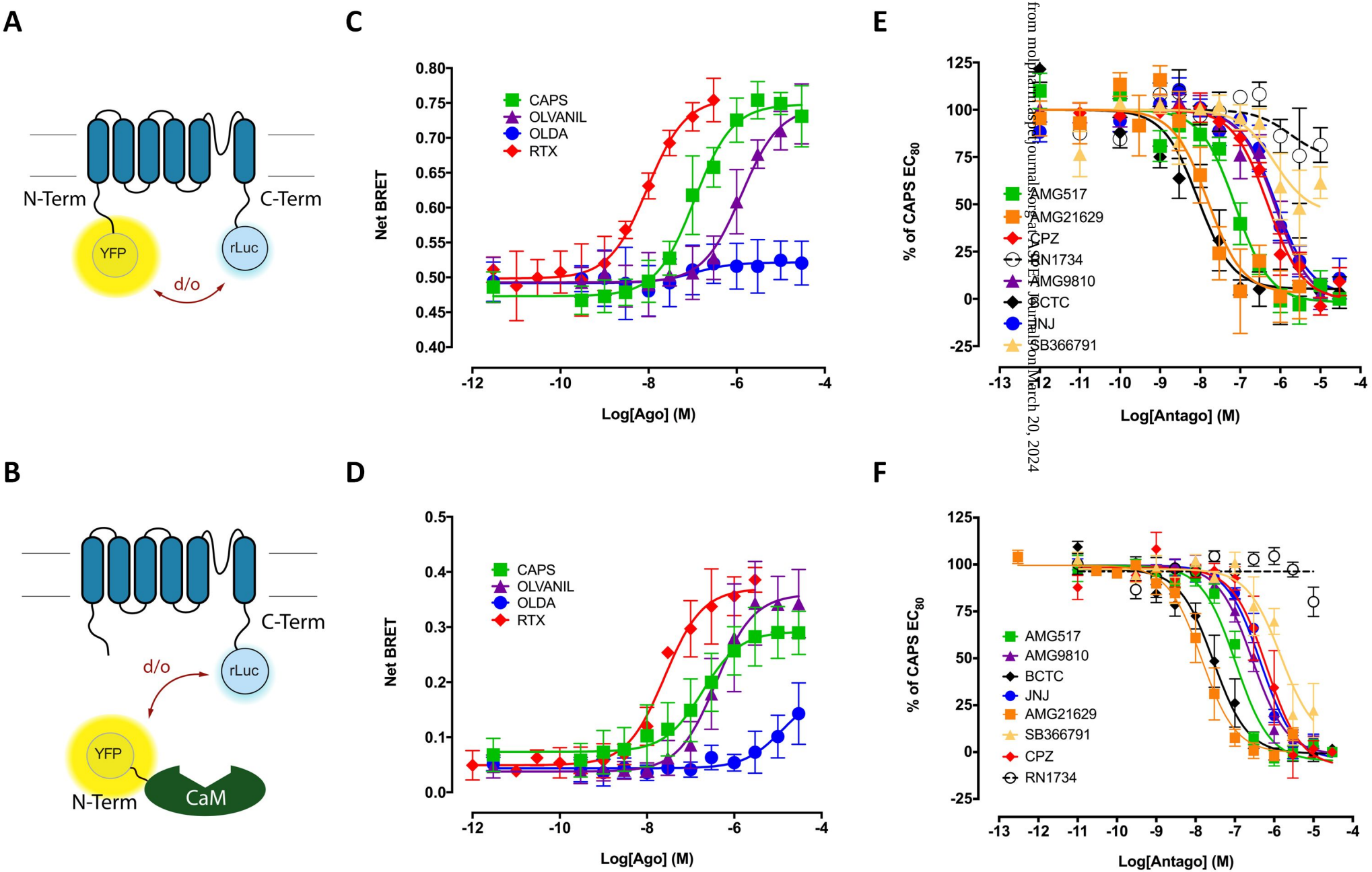

Figure 1

ed from molpharm.aspetjournals.org at ASPET Journals on March 20, 2024

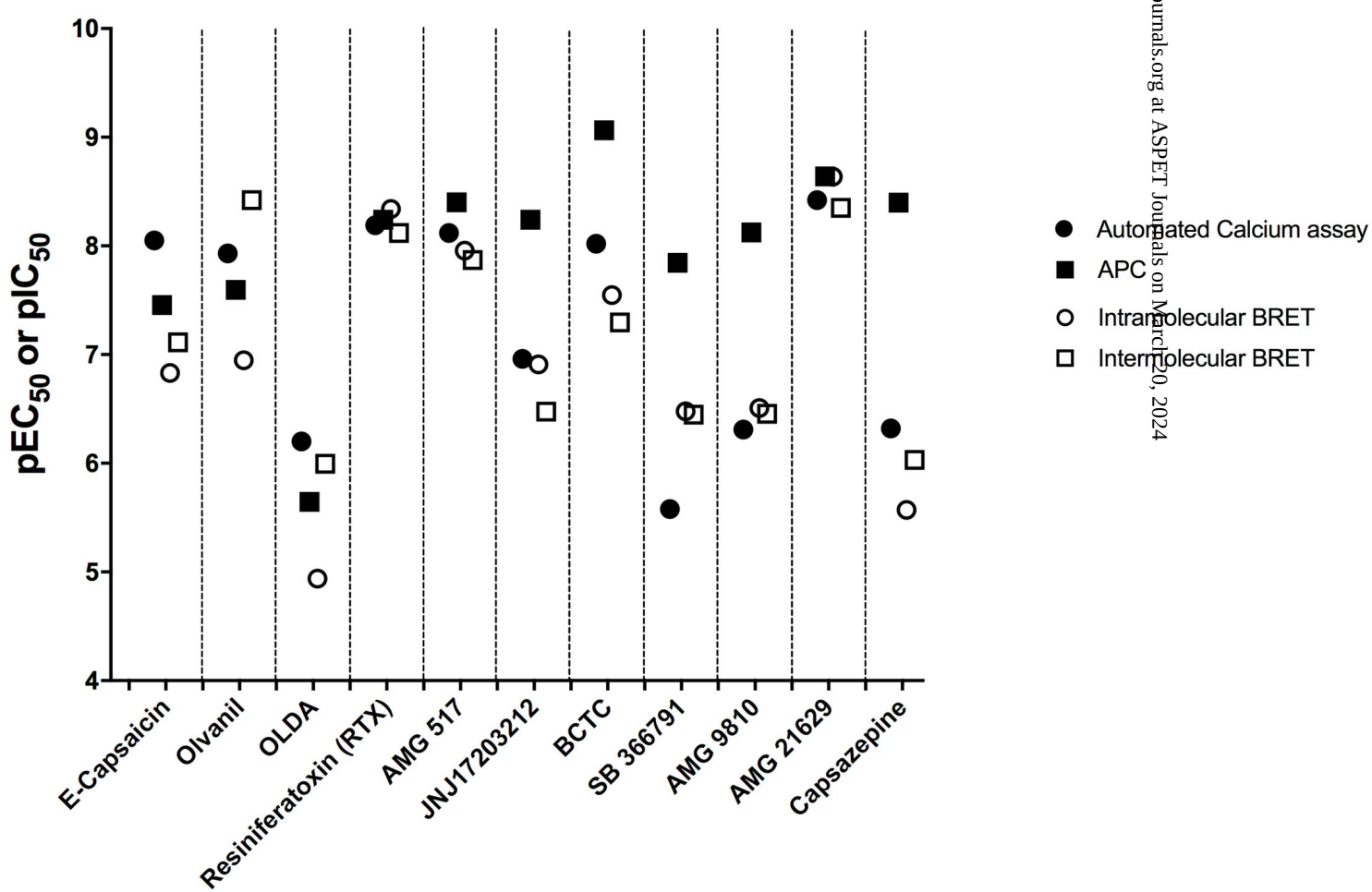

ed from molpharm.aspetjournals.org at ASPET Journals on March 20, 2024

Figure 2

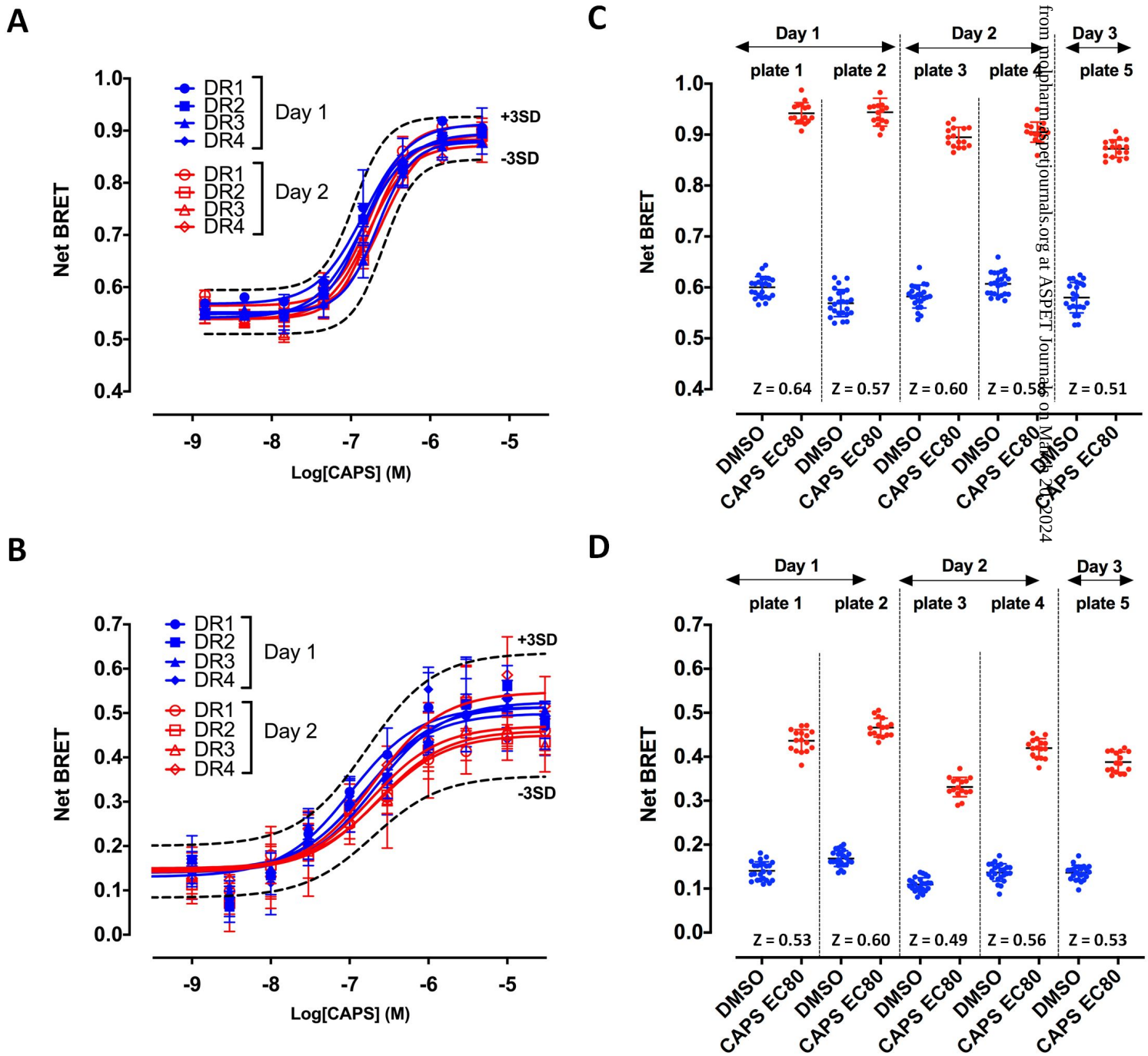

Figure 3

ed from molpharm.aspetjournals.org at ASPET Journals on May 20, 2024

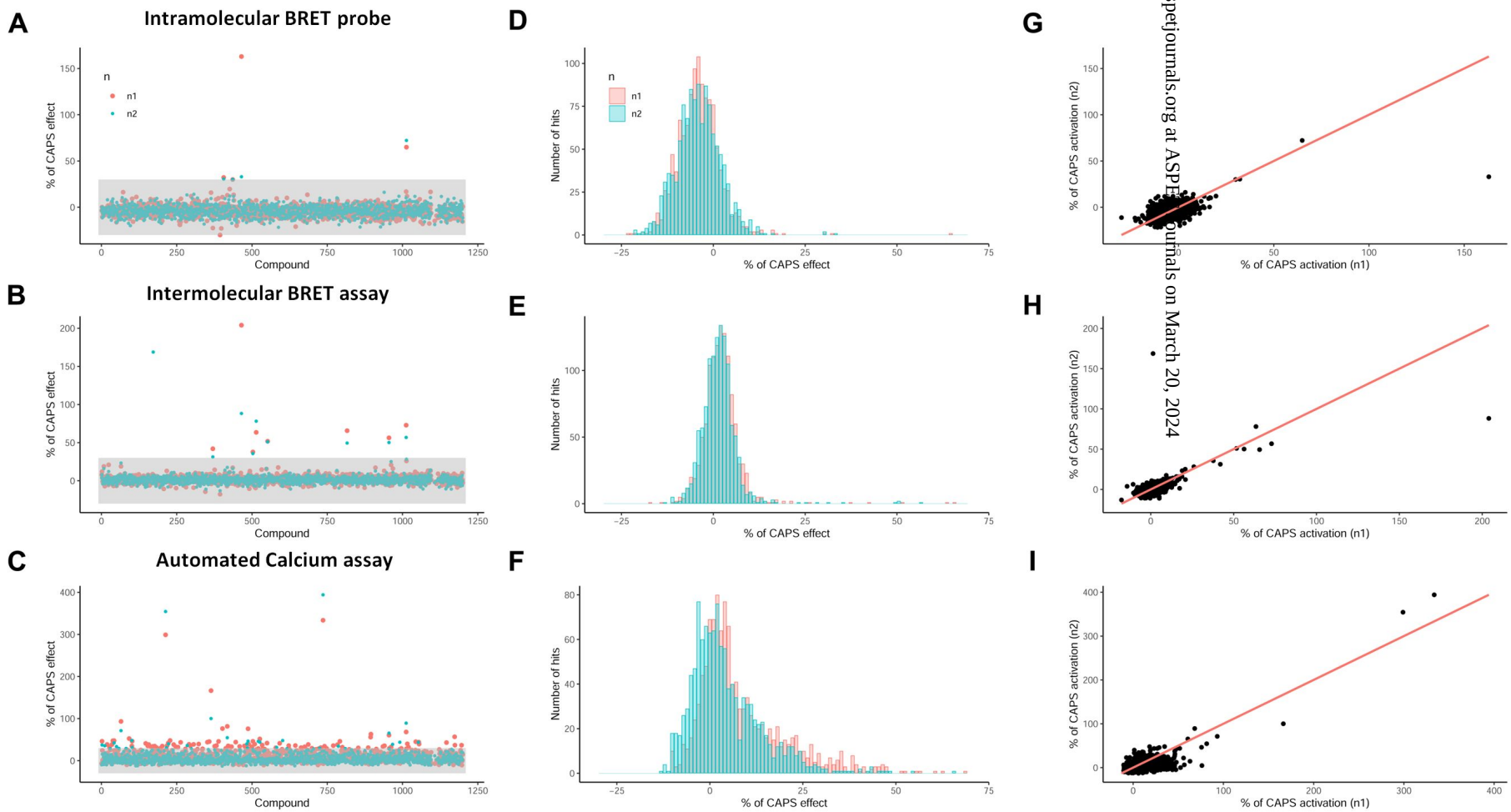

ed from molpharm.aspetjournals.org at ASPET Journals on March 20, 2024

Figure 4

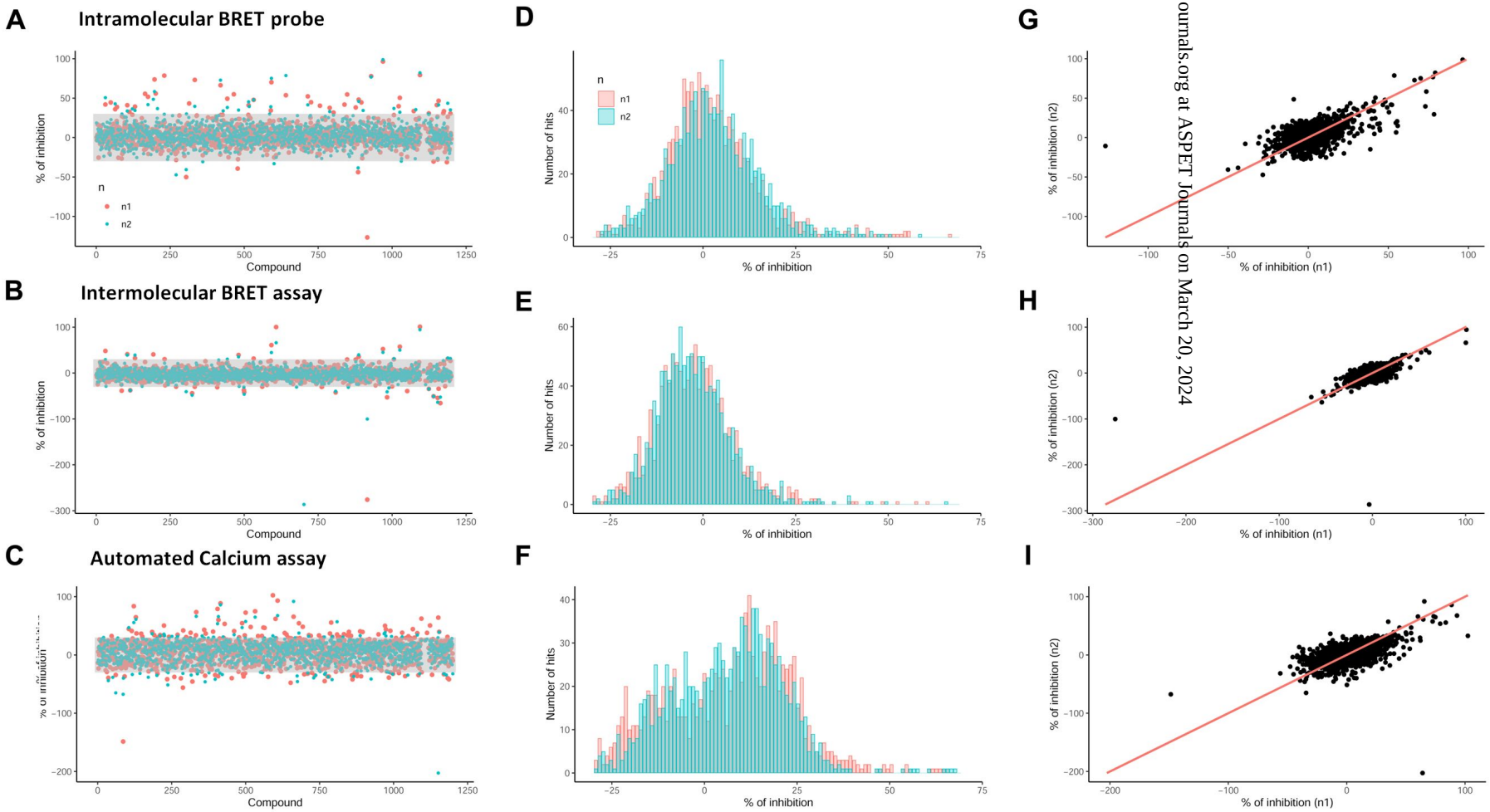

Figure 5

ed from molpharm.aspetjournals.org at ASPET Journals on March 20, 2024

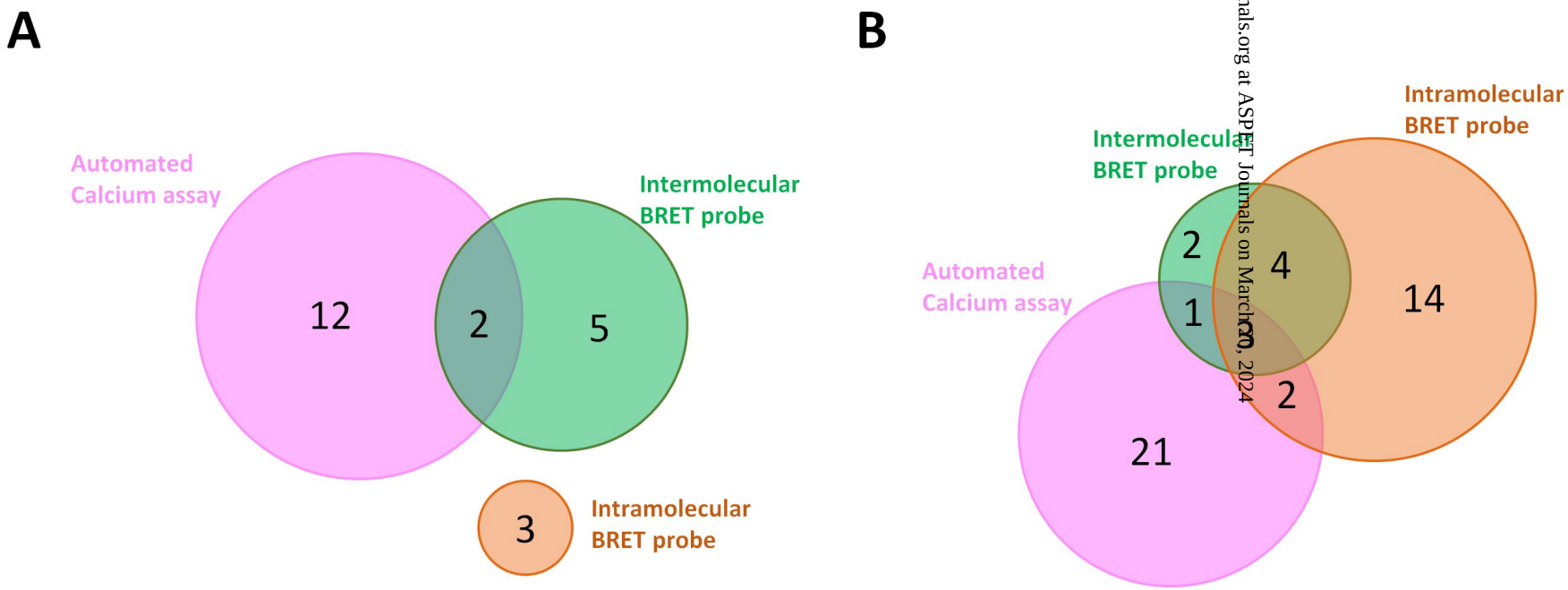

Figure 6

ed from molpharm.aspetjournals.org at ASPET Journals on March 20, 2024

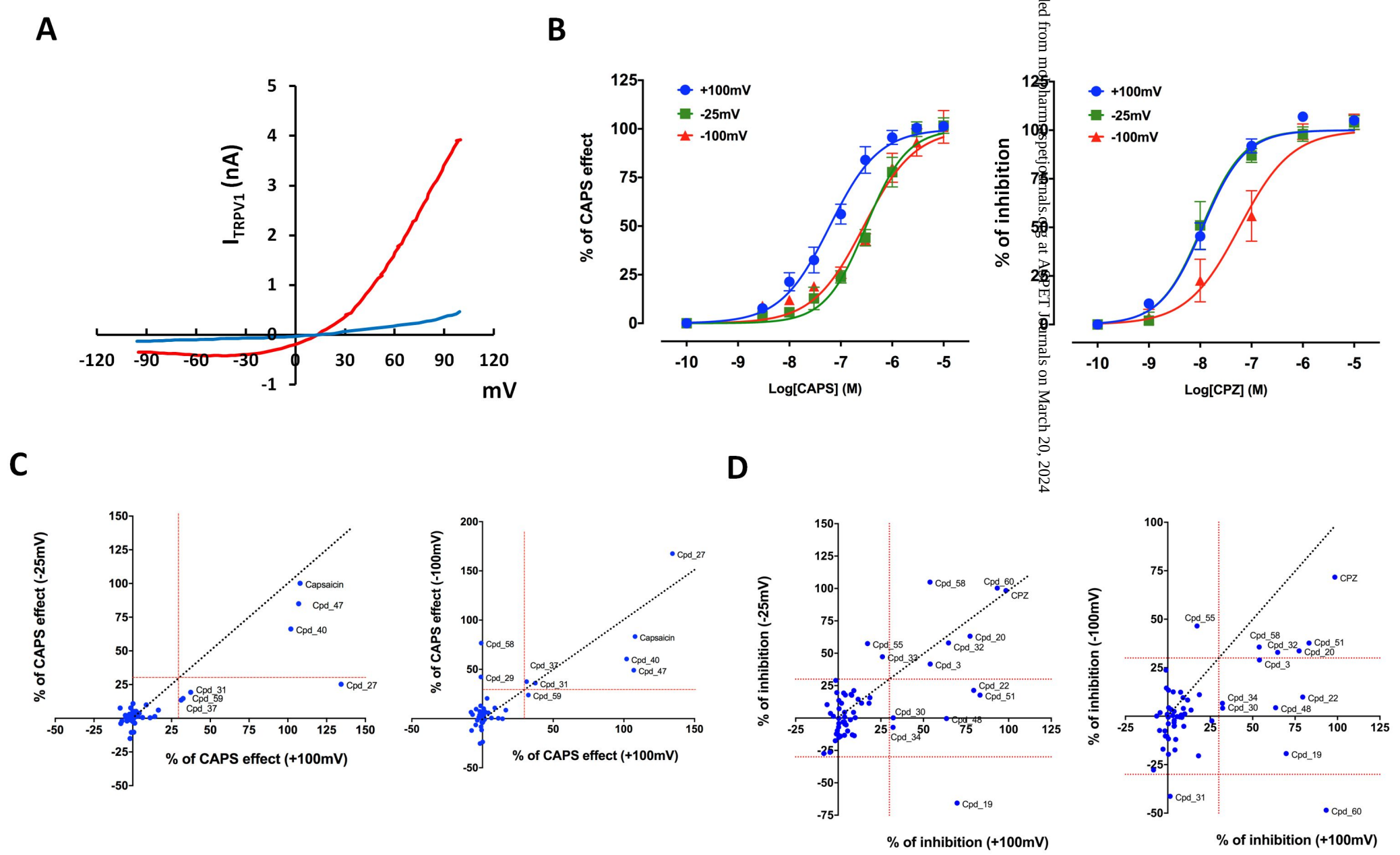

Figure 7

Downloaded from molpharm.aspetjournals.org at ASPET Journals on March 20, 2024

			Activation mode						Inhibition mode					
Compound	CLUSTER	Biblio. Indication	BRET INTRA	BRET INTER	CALCIUM	APC 100mV	APC -25mV	APC -100mV	BRET INTRA	BRET INTER	CALCIUM	APC 100mV	APC -25mV	APC -100mV
47	I			X		X	X	X	X		X			
27	C			X	X	X		X			X			
18	E	Cam_Inh		X	X	X			X		X			
40	F			X		X	X	X		X*		X*	X*	X*
37	D			X	X	X		X		X*	X*			
22	G	Cam_Inh			X							X		
52	E		X						X*		X*			
45	NC		X								X			
31	I				X	X		X			X			X*
19	E										X	X	X*	
59	I				X	X					X			
15	A										X			
24	F									X*	X			
17	NC				X					X*	X			
29	NC							X		X*	X			
41	F			X										
14	F				X									
53	F				X									
16	A										X			
57	F										X			
43	F										X			
36	H								X					
13	H								X					
46	E								X					
12	NC	Cam_Inh									X			
11	E	Cam_Inh			X						X			
30	G				X	X						X		
5	G	Cam_Inh									X			
26	S										X			
21	S										X			
44	G				X						X*			
9	C				X									
50	C				X						X			
28	J	Cam_Inh							X					
25	E	p_Cam_Inh							X					
33	J	p_Cam_Inh							X				X	
7	A										X			
1	G	Cam_Inh							X	X				
3	G	Cam_Inh									X	X	X	
55	C									X			X	X
51	F								X			X		X
32	E	Cam_Inh							X			X	X	X
20	E	Cam_Inh							X			X	X	X
54	G								X	X				
23	G	Cam_Inh							X					
56	J	p_Cam_Inh							X					
35	E	p_Cam_Inh							X	X				
8	E	p_Cam_Inh								X	X			
4	G	Cam_Inh							X	X	X			
6	G	Cam_Inh							X	X	X			
34	E								X			X		
48	E	p_Cam_Inh		X					X			X		
2	F				X				X		X			
58	F							X	X*		X	X	X	X

Figure 8

Downloaded from molpharm.aspetjournals.org at ASPET Journals on March 20, 2024

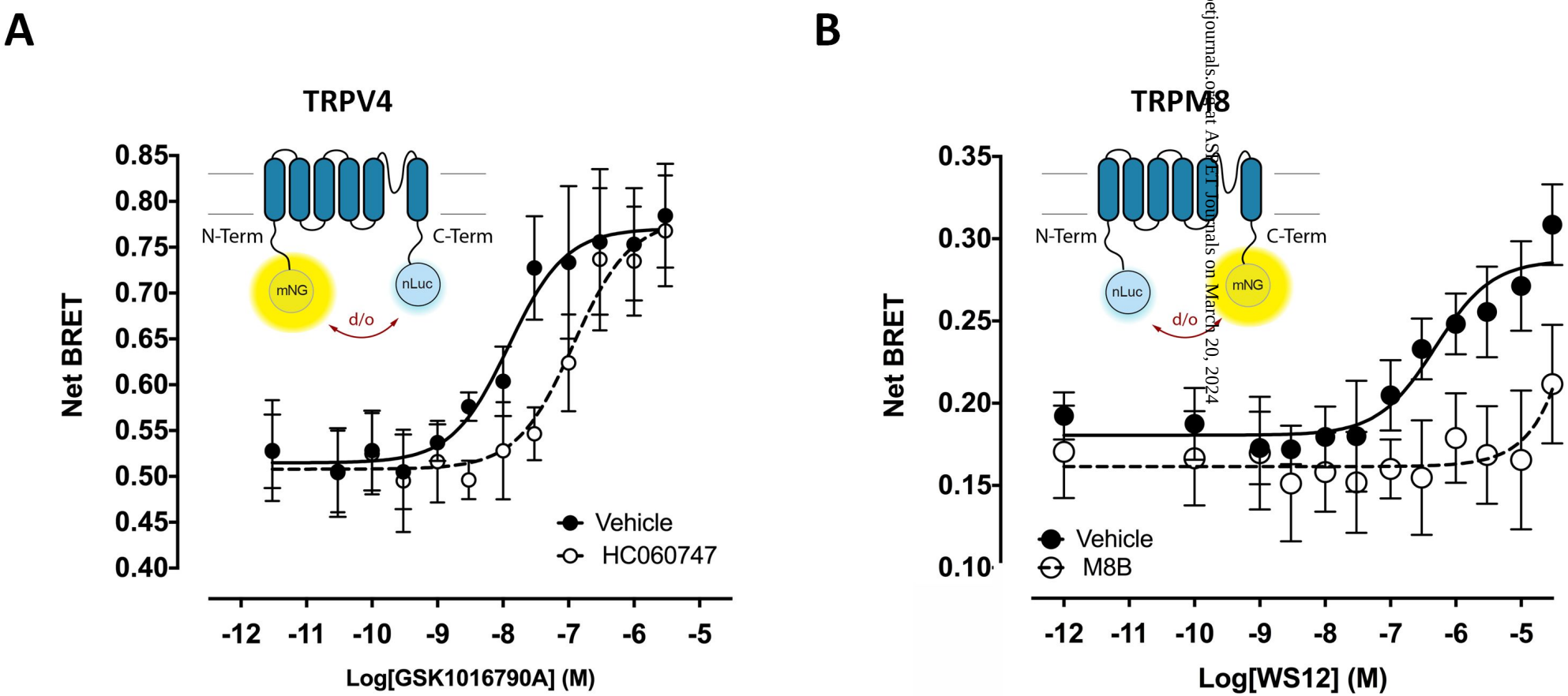

ed from molpharm.aspetjournals.org at ASPET Journals on March 20, 2024

Figure 9

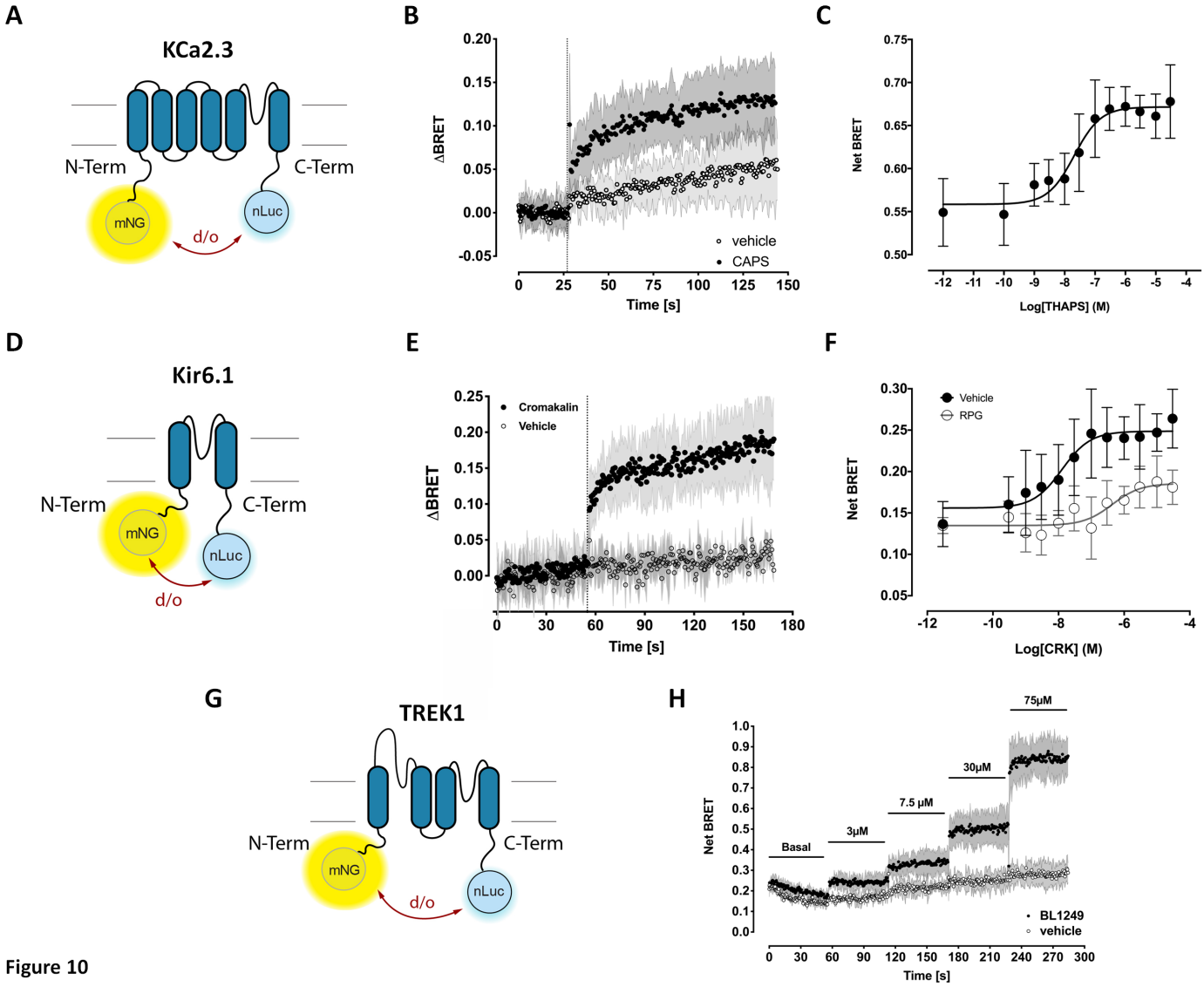

Figure 10

Downloaded from molpharm.aspetjournals.org at ASPET Journals on March 20, 2024

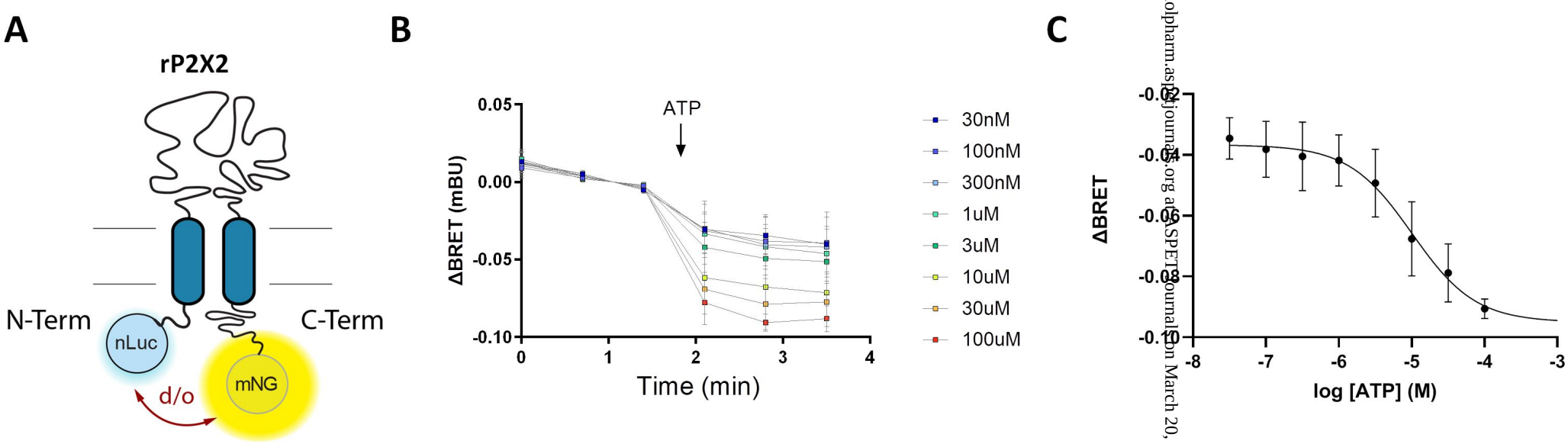

ed from molpharm.aspetjournals.org at ASPET Journals on March 20, 2024

Figure 11